

# Acoustic Function of Sound Hole Design in Musical Instruments

by

Hadi Tavakoli Nia

Submitted to the Department of Mechanical Engineering  
in partial fulfillment of the requirements for the degree of

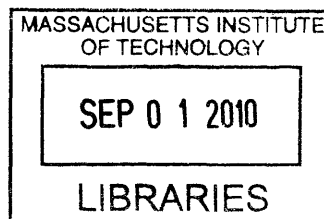
Master of Science in Mechanical Engineering

at the

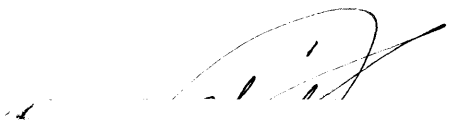
MASSACHUSETTS INSTITUTE OF TECHNOLOGY

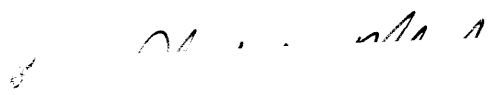
June 2010

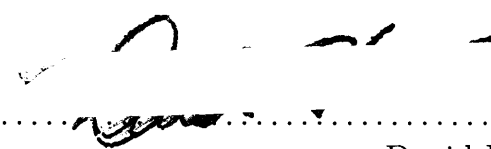
**ARCHIVES**



© Massachusetts Institute of Technology 2010. All rights reserved.

Author  .....  
Department of Mechanical Engineering  
May 22, 2010

Certified by  .....  
Nicholas C. Makris  
Professor  
Thesis Supervisor

Accepted by  .....  
David E. Hardt  
Chairman, Department Committee on Graduate Theses



# Acoustic Function of Sound Hole Design in Musical Instruments

by

Hadi Tavakoli Nia

Submitted to the Department of Mechanical Engineering  
on May 22, 2010, in partial fulfillment of the  
requirements for the degree of  
Master of Science in Mechanical Engineering

## Abstract

Sound-hole, an essential component of stringed musical instruments, enhances the sound radiation in the lower octave by introducing a natural vibration mode called air resonance. Many musical instruments, including those from the violin, lute and oud families have evolved complex sound-hole geometries through centuries of trial and error. However, due to the inability of current theories to analyze complex sound-holes, the design knowledge in such sound-holes accumulated by time is still uncovered. Here we present the potential physical principles behind the historical development of complex sound-holes such as rosettes in lute, f-hole in violin and multiple sound-holes in oud families based on a newly developed unified approach to analyze general sound-holes. We showed that the majority of the air flow passes through the near-the-edge area of the opening, which has potentially led to the emergence of rosettes in lute family. Consequently, we showed that the variation in resonance frequency and bandwidth of different traditional rosettes with fixed outer diameter is less than a semitone, while the methods based on the total void area predicts variations of many semitones. Investigating the evolution of sound-holes in violin family from circular geometry in at least 10th century to the present-day f-hole geometry, we found that the evolution is consistent with a drive toward decreasing the void area and increasing the resonance bandwidth for a fixed resonance frequency. We anticipate this approach to be a starting point in discovering the concepts behind the geometrical design of the existing sound-hole geometries, and helping the musicians, instrument makers and scientists utilize this knowledge to design consistently better instruments.

Thesis Supervisor: Nicholas C. Makris  
Title: Professor



## Acknowledgments

First, I would like to thank my thesis advisor, Prof. Nicholas C. Makris, for his guidance and insight. Professor Makris will always be a model for me in his problem identification and problem solving skills, his discipline in leading and guiding the projects and his skill in professional scientific communications and presentation.

Second, I would like to thank Dr. Mohammad-Reza Alam for his presence, guidance and support in all stages of the project, to name one, the memorable test we did at 2 am, in minus 20 degree C on New Year's Eve.

Many individuals contributed in developing the computational models, experimentation and fabrication including Dr. Yuming Liu in Mechanical Engineering Department, Amit Zoran in Media Lab, Marianne Ganzer of Johnson string, Darcy Kuronen of Museum of Fine Art and Roman Barnas of North Bennet Street School.

The administrative staff at MIT were extraordinary in their support. In particular I thank Leslie Regan, Joan Kravit and Geoffrey Fox.

My fellow students and friends provided advice, support, critique and conversation for which I am most grateful. I would like to thank Srinivasan Jaganathan, Ioannis Bertsatos, Tianrun Chen, Deanelle Symonds, Alex Tan, Ankita Jain, Anamaria Ignisca, Reza Sharifi Sedeh, Francesco Mazzini, Vedran Sohinger, Shani Sharif, Marmar Mehrabadi and Saeed Bagheri.

Finally, I am grateful to have been awarded the Office of Naval Research Graduate Traineeship Award in Ocean Acoustics for part of my Master program.

To my family, I am forever grateful for all the love, support, and patience it took to get me this far.

# Contents

<b>1</b>	<b>Introduction</b>	<b>17</b>
<b>2</b>	<b>Method</b>	<b>21</b>
<b>3</b>	<b>Experimental Setup</b>	<b>25</b>
<b>4</b>	<b>Lute Rosette</b>	<b>29</b>
<b>5</b>	<b>Violin f-hole</b>	<b>33</b>
<b>6</b>	<b>Multiple Sound-holes</b>	<b>39</b>
<b>7</b>	<b>Conclusion</b>	<b>41</b>
<b>A</b>	<b>Figures</b>	<b>43</b>
<b>B</b>	<b>Tables</b>	<b>67</b>





# List of Figures

- A-1 Schematic of an opening. The potential  $\phi = 0$  on the opening surface,  $\partial\phi/\partial n = 0$  on the baffle and  $\phi \rightarrow 0$  as the distance from the center of the opening  $|\mathbf{r}| \rightarrow \infty$ . . . . . 44
- A-2 The error in validation of the numerical scheme for calculating the conductance of a circular opening. The error percentage, calculated as  $e = (C_{numerical} - C_{analytical})/C_{analytical} \times 100$  is shown versus  $n$  the number of element on each side (i.e., the pattern is digitized as  $n \times n$  grid and the total number of elements is  $N = n^2$ ). . . . . 45
- A-3 Resonator setup is shown. The resonance box is made of a cardboard with thickness of 5 mm, and top and back plates out of plywood with thickness of 7 mm. The pattern is carved on a 3-mm plywood and mounted on the top plate. The contact between the top and back plates and the cardboard are sealed with rubber tapes. The microphone as the receiver is placed inside the resonance box attached to the back plate. The speaker is placed in front of the pattern. . . . . 46
- A-4 Opening patterns: (a) Lute rose (Wendelin Tiffenbrucker [1]), (b) Lute rose (Warwick Hans Frei [1]), (c) Theorbo rose [1], (d) Violin f-hole, (e) Oud rose (pattern removed) and (f) sound-hole in the form of a ring. 47

- A-5 Air resonance curves of f-hole are shown for  $n = 9$  measurements (gray curves). The sound level is normalized by the peak level. Each curve is smoothed by window averaging with window width of 1000 samples. The black line represents the average of the nine measurements. The horizontal dotted line represents the 3-dB and 10-dB down level from the peak. Frequencies  $f_1$  and  $f_2$  are where the 3-dB down level cuts the curve. The peak frequency is then obtained as  $f_0 = (f_1 + f_2)/2$ . . . . . 48
- A-6 Measuring the decay slope of the amplitude of the pressure inside the box provides a different method to calculate the 3-dB down bandwidth of the resonance curve shown in Fig. A-5. The slope  $\alpha$  is measured during the free oscillation of the resonator after the excitation source is removed (in this figure, after 5.65 s). The 3-dB down bandwidth  $\Delta f$  is then obtained as  $\Delta f = -\frac{\alpha}{\pi}$ . The reference pressure  $P_0$  is set to  $P_0 = 1$ . The slope  $\alpha$  is independent of the value of  $P_0$ . . . . . 49
- A-7 The volume of the sound box is measured by first assuming the top and back plates to be flat and then correct this assumption by a correction factor obtained by filling the volume with sand. The flat area of the top and back plate and the height of the box is measured in AutoCAD by inserting the images of each instrument. . . . . 50
- A-8 The cavity volume is measured by filling the violin with sand. . . . . 51
- A-9 The air resonance of the following lute rosettes is characterized: (a) Wendelio Venere 1592 (b) Hans Frei 1 1540 (c) in Padov 1595 (d) Sebastian Schelle 1744 (e) Hans Frei 2 1540 (f) Wendelin Tieffenbrucker 1590. Comparing the resonance frequency due to each rosettes, we observed a variation within 30 percent of a semitone. With center frequency of 123 Hz used in the experiment, the 3-dB-down bandwidth variation stays within eight percent of a semi-tone. It should be mentioned that the outer diameters and thicknesses of all the rosettes and the experimental setup such as the box volume, microphone and speaker placements were the same in the above comparison. . . . . 52

A-10 (a) The radial distribution of the void area, (b) the angular distribution of the void area used as the lower and upper limits for the resonance frequencies of the discussed lute rosettes (Fig. A-11). The radial distribution is composed of nine rings with equal widths. To increase the void area, the width of each ring is equally increased. The angular distribution is composed of 20 sectors with equal angles. To increase the void area, the angle of each sector is increased equally. . . . . 53

A-11 Comparing the resonance frequencies of different lute rosettes to radial and angular hole distributions (Fig. A-10). The frequency  $f_0$  and the area  $A_{total}$  represent respectively the resonance frequency and the area of a circular opening with the same diameter of the outer diameter of lute rosettes studied. . . . . 54

A-12 Resonance frequency of a ring with different ratio between the outer and inner diameters is shown. The diameter of the inner and outer circles are shown by  $d$  and  $D$ , respectively. The frequency  $f_0$  corresponds to the resonance frequency of an opening with diameter  $D$  ( $d=0$ ). The vertical axis on the right are scaled on semitones (In diatonic system, each octave is divided into 12 equidistant intervals called semitone. So, each semitone is  $2^{1/12}$  of an octave). The results show that the resonance frequency is highly dependent on the outer periphery of the opening. . . . . 55

A-13 Flux distribution profile in log scale,  $\log(\sigma)$  (the source strength  $\sigma$  is obtained from Eq. 2.9) is shown for Warwick Hans Frei lute. The flux is normalized by its maximum value, so the zero value in the colorbar represents the maximum flux value. . . . . 56

A-14 The rosette on Andreas Berr lute. The image is taken from the website of Stephen Barber and Sandi Harris, lute makers [1]. . . . . 57

A-15	The spectrum of the Andreas Berr lute at low frequencies. The sound level is normalized by the peak level. The air resonance frequency corresponding the peak shown was measured at 124 Hz. The blue curve shows the raw data, and the red line shows the process data after taking Fourier Transform. The asymmetry of the resonance curve is due to the reflection of sound from the walls. . . . .	58
A-16	The line of development of sound-holes in violin is shown for circular opening (a) in 10th-century viols [8] (A), semi-circular opening (b) in Lyras in 13th century [8] (B), crescent (c) [16] and semi-circular strip (d) [20] in 13th century instruments (C), primary c-hole (e) [20] [20] and c-hole (f) in early viols and violins (D,E) in 16th century [5] and present-day f-hole (g) in violins (F) staying unchanged since 17th century [5]. The 10-dB down bandwidths of air resonance of the above openings are shown for a fixed resonance frequency (solid line). The 10-dB-down bandwidth of resonance curve increases monotonically from circular opening to f-hole up to a semitone. The opening area (dotted line), normalized by the area of the present-day f-hole, is reduced by a factor of two from circular opening to c-hole and f-hole. . . . .	59
A-17	The sound spectrum of four famous Cremonese violins from Martin Schleske's website [2]. The air resonance at around 270 Hz shows that a 10-dB down bandwidth is more appropriate than the more standard 3-dB down bandwidth. . . . .	60
A-18	The drawing of the Emiliani Stradivari of 1703 from which the expression for air resonance frequency is obtained [5]. . . . .	61

A-19 The effectiveness of the developed approach is shown by applying it to obtain exact air resonance frequency in violin family. The results using general sound-hole theory (in blue) are compared to the results using circular sound-hole theory (in black). A correction factor is used to for each member of the family to scale the circular theory data to its corresponding experimental data. The numbers below the figure shows the conventional sizes of each instrument. . . . . 62

A-20 The effect of the distance between f-holes on air resonance frequency. The resonance frequency  $f$  is normalized by  $f_0$ , the air resonance frequency of an f-hole geometry the same as Stradivari of 1703 (Fig. A-18). The distance  $d$  is normalized by  $d_0$ , the distance between f-holes of the same violin. The horizontal dotted lines shows one semi-tone higher and lower than the reference frequency. The change in distance by a factor of two results in resonance frequency variation of less than a semi-tone. . . . . 63

A-21 Flux distribution profile in log scale,  $\log(\sigma)$  (the source strength  $\sigma$  is obtained from Eq. 2.9) is shown for f-hole. The flux is normalized by its maximum value, so the zero value in the colorbar represents the maximum flux value. The irregular shape of f-hole results in higher rate of flux at the necks. The consequent effect is an increase in viscous damping and consequently, an increase in resonance bandwidth. The flux is normalized by the maximum velocity. . . . . 64

- A-22 The distance between the holes  $D$ , normalized by a reference distance  $D_0$  in standard theorbos and ouds, is varying having the hole diameters  $d$  fixed. For theorbo, the upper three circles,  $D_0 = 1.24d$ , and for oud, the lower three circles,  $D_0 = 1.39d$ . The frequencies  $f$  and  $f_0$  represent the corresponding resonance frequencies. The resonance frequencies of theorbo and oud ( $D_0/D = 0$ ), obtained via the developed method, is compared with the superposition approximation, which is equivalent to the case that the holes are infinitely far ( $D_0/D \rightarrow 0$ , shown by the arrows). The lower and upper sketches represent the oud and theorbo sound-holes, respectively. The arrows  $a$  and  $b$  indicate the resonance frequencies when the holes are infinitely far from each other. In this case, using superposition to calculate the resonance frequency is valid. 65
- A-23 Flux distribution profile in log scale,  $\log(\sigma)$  (the source strength  $\sigma$  is obtained from Eq. 2.9) is shown for oud sound-hole. The flux is normalized by its maximum value, so the zero value in the colorbar represents the maximum flux value. . . . . 66

# List of Tables

B.1	The error obtained using Eq. 5.4 based on the semi-empirical Eq. 5.1. Each instrument shown in the table is the one used to find the parameter $a$ in Eq. 5.1. The resonance frequencies of other instruments of the family is then obtained based the same value of $a$ . . . . .	67
-----	--	----





# Chapter 1

## Introduction

Air resonance in musical instruments boosts the sound radiation at low frequencies where the corpus suffers from absence of natural modes [14]. Studies of the fundamental air resonance, also referred to as Helmholtz, cavity and A0 resonance, has been initiated by Savart [17], Helmholtz [23, 22], Rayleigh [15] and Lamb [12] by formulating the resonance frequencies of the resonators with simple circular and elliptical openings. However, many musical instruments, including those from the violin, lute and oud families, have evolved far more complex sound-hole geometries. Existing methods for characterizing the air resonance in such instruments rely on approximating the complex sound-holes by simple circular and elliptical geometries for which the analytical solutions are available [9, 6, 18]. For example, f-hole geometry is approximated as an elliptical hole matching the sinuate slot, and two circular holes matching the ends [6, 18, 10]. The error due to this approximation is usually corrected by empirical fitting factors [4]. In the aforementioned approximate methods, the air resonance frequency is assumed to be proportional to the square root of the void area, which is not a valid approximation as will be shown in this paper. These methods also suffer from being case dependent and complicated because of the need to the correction factors. A unified theory for exact calculation of the air resonance frequency in instruments with complex sound-holes is missing in the literature [4]. A general theory can provide the analysis tools to pass on and interpret the knowledge in instrument making, which is accumulated and evolved over centuries. Additionally,

a theoretical method for determining the air resonance characteristics in stringed instruments can help the instrument makers improve the instrument design by avoiding empirical trial and error methods.

We developed a general method for numerical calculation of the air resonance frequencies of instruments with complex sound-holes such as the one in violin, lute and oud families. For this purpose, we found it necessary to go back to fundamental theories on resonators by Rayleigh [15]. Applying our method on lute rosettes, we showed that the majority of the air flow passes through near-the-edge area of the opening, and consequently, the central part of such sound-holes contributes least to the air resonance. This fact has been validated by measuring the resonance frequency of resonators with sound-holes as circular rings of varying inner diameter. As a result, the resonance frequency of lute rosettes with the least void area (e.g. Hans Frei rosettes) measured to vary within a semitone compared to circular sound-holes (e.g. in guitar) with the same outer diameter. Measuring the resonance characteristics of several different traditional lute rosettes, we observed that the variation in resonance frequencies and bandwidths are less than one third of a semitone, much smaller than the square root of the variation in the corresponding hole areas (used by conventional methods) for a fixed outer diameter. Different roles such as improving the aesthetic of the instrument, covering the sound bar and saving the soundboard wood can be attributed to the appearance of the traditional lute rosettes, potentially evolved through centuries to have low variation in resonance frequency and bandwidth. The low dependence of resonance characteristics on rosette patterns provides an ease of calculation for lute makers by only measuring the outer diameter.

Economy of void and increase in the bandwidth of air resonance curve have potentially been the driving forces in the evolution of sound-hole geometry in violin family. A systematic analysis of the sound-holes in violin ancestors shows a line of development tracing back to circular openings toward the present-day f-hole geometry as it follows: circular sound-holes in early viols observed first in 10th century[8], semi-circular sound-hole in the later ancestors of the violin such as Lyras in 13-th century [3], crescent-shape sound-holes [16], semi-circular strips [20] and c-holes [20]

in early viols and violins of 16th century [5] and eventually to the present-day f-holes stayed unchanged since 17th century [5]. Applying the method developed, we showed that acoustic effects are consistent with this evolution process. For a given resonance frequency, we observed an increasing trend in resonance bandwidth and a decreasing trend in the void area of the chronological order mentioned above, which are both favorable for the sound quality.

The increase in bandwidth, observed in the evolution of sound-hole in violin family, enhances a wider range of frequencies at low-frequency region of the spectrum where the absence of modes is well-known [14]. The increase in bandwidth is also favorable to the instrument maker by giving more tolerance in placing the air resonance. We also showed that the economy of wood can be another driving force in sound-hole evolution in violin family. Comparing the two endpoints of the evolution process, circular and f-hole geometries, at a fixed air resonance frequency, we observed a reduction of missing wood by a factor of two. The conventional methods, which are based on void area, would have ignored this fact on efficiency of f-hole in saving wood area. The saved amount of wood can contribute in more efficient radiation of sound from the sound board by increasing the radiating area and saving the vertical fibers of the soundboard. Additionally, changing from circular to more stretched shape such as f-hole suggests conformity to the violin corpus geometry to avoid interference with the main mode of the sound board at low frequencies.



# Chapter 2

## Method

Assuming the dimensions of the resonance box and the opening are much smaller than the sound wavelength at resonance frequency, the equation governing air flux through the opening (Fig. A-1) is given by (Eqs. 2.1-2.4 are derived by Lord Rayleigh [15]):

$$\frac{d^2U}{dt^2} + \tilde{C}\frac{c_0^2}{V}U = 0 \quad (2.1)$$

where  $U$  is the volume of the air passing through the opening,  $c_0$  the sound speed,  $V$  the volume of the resonance box,  $\tilde{C}$  the conductance of the opening, and  $t$  the time. The resonance frequency of the opening is then obtained as,

$$f = \frac{c_0}{2\pi} \sqrt{\frac{\tilde{C}}{V}} \quad (2.2)$$

In the above,  $\tilde{C}$  is an intrinsic property of the opening and depends on the geometry of the opening only. For an opening with cross-sectional area  $A$  and wall thickness  $h$ , we have:

$$\frac{1}{\tilde{C}} = \frac{1}{C} + \frac{h}{A} \quad (2.3)$$

where the first term on the right-hand side represents the geometry effect of the opening and the second term represents the thickness effect. The conductance for the infinitely thin opening,  $C$ , is obtained generally by a potential flow problem. The

associated boundary-value problem for the potential function  $\phi$  consists of the field equation,  $\nabla^2\phi = 0$ , and the boundary conditions:

- (i)  $\phi=1$  on the opening surface  $S$
- (ii)  $\partial\phi/\partial n=0$  on the baffle (where  $n$  is the outward normal direction of the boundary surface )
- (iii)  $\phi \rightarrow 0$  as the distance from the center of the opening  $|\mathbf{r}| \rightarrow \infty$ .

In terms of the normal velocity of the flow at the opening,  $C$  is given by

$$C = \frac{1}{2} \iint_S \frac{\partial\phi}{\partial n} ds \quad (2.4)$$

The same expression for conductance can also be obtained from an alternative set of boundary conditions:

- (i)  $\phi=0$  on the opening surface  $S$
- (ii)  $\partial\phi/\partial n=0$  on the baffle (where  $n$  is the outward normal direction of the boundary surface )
- (iii)  $\phi^+ \rightarrow 1$  and  $\phi^- \rightarrow -1$  where  $\phi^+$  is the potential at far infinity on the upper side of the opening shown in Fig. A-1 and  $\phi^-$  is the potential at far infinity on the lower side of the opening (In Fig. A-1 only  $\phi^+$ , the potential on the upper side is schematically shown).

The conductance is then given by

$$C = \frac{\iint_S \frac{\partial\phi}{\partial n} ds}{\phi^+ - \phi^-} \quad (2.5)$$

Replacing the value of the potentials in the denominator, which is equal to  $\phi^+ - \phi^- = 2$ , explains the coefficient of  $\frac{1}{2}$  in Eq. 2.4.

For the special case of circular and elliptical openings, the above boundary-value problem can be solved analytically [12]. For a circular opening with radius  $R$ , in particular, we have  $C=2R$ . This is usually used to approximate the conductance of openings with complex geometries based on equivalent circular opening areas. In this

study we develop an effective and robust approach to obtain the exact solution of  $\phi$  for an opening of arbitrary geometry. To do that, we apply the so-called source method in which a source distribution with (unknown) strength  $\sigma(\mathbf{r})$  is distributed over the opening surface  $S$ . The resulting potential is

$$\phi(\mathbf{r}) = \iint_{S(\mathbf{r}')} \sigma(\mathbf{r}') G(\mathbf{r}; \mathbf{r}') ds' \quad (2.6)$$

where  $G(\mathbf{r}; \mathbf{r}') \equiv 1/|\mathbf{r} - \mathbf{r}'|$  is the Rankine source Green function [11]. The potential  $\phi$  in (2.6) satisfies all the conditions of the boundary-value problem except the boundary condition (i). The imposition of this condition leads to an integral equation for unknown  $\sigma(\mathbf{r})$ :

$$\iint_{S(\mathbf{r}')} \sigma(\mathbf{r}') G(\mathbf{r}; \mathbf{r}') ds' = 1 \quad (2.7)$$

In terms of  $\sigma(\mathbf{r})$ , we have

$$C = \frac{1}{4} \iint_S \sigma(\mathbf{r}) ds \quad (2.8)$$

where use has been made of Eq. 2.4 and the fact that the flux passing through the surface  $S$  is half of the source strength  $\sigma$ . Since the sources are distributed on the infinitely thin surface  $S$  (Fig. A-1), half of the flux of the source is flowing above the surface  $S$  (the direction of our interest) and the other half is flowing down the surface  $S$ . So, the flux  $\partial\phi/\partial n = \sigma/2$ .

To solve the integral equation (2.6), we apply the constant panel method. To do that, we divide  $S$  into  $N$  quadrilateral (or triangle) elements,  $S_j$ ,  $j=1, 2, \dots, N$ , and approximate  $\sigma(\mathbf{r})$  on  $S_j$  by the constant value  $\sigma_j = \sigma(\mathbf{r}_j)$  where  $\mathbf{r}_j$  represents the center of  $S_j$ . With these, (2.7) becomes

$$\sum_{j=1}^N P_j(\mathbf{r}) \sigma_j = 1, \quad \mathbf{r} \in S \quad (2.9)$$

where the influence coefficient  $P_j$  is given by

$$P_j(\mathbf{r}) = \iint_{S_j(\mathbf{r}')} G(\mathbf{r}; \mathbf{r}') ds', \quad j = 1, 2, \dots, N \quad (2.10)$$

Imposition of (2.9) at the centers of the  $N$  elements leads to a system of  $N$  linear equations from which the  $N$  unknowns,  $\sigma_j$ ,  $j = 1, 2, \dots, N$ , can be obtained. With this method, the numerical error associated with the discretization vanishes with increasing  $N$  as at least  $N^{-1/2}$ .

In order to validate the numerical scheme, we obtained the conductance of a circular opening numerically and compared it with analytical results. For circular opening the conductance is available analytically and is equal to the diameter of the circle. The error percentage falls to less than one percent when we use the number of element more than  $60 \times 60$  (Fig. A-2).



# Chapter 3

## Experimental Setup

The experimental setup comprises of a resonance box with variable volume and replaceable top plate. The resonance box is made of a thick cardboard cylinder with changeable diameter and height, confined with top and back plates (Fig. A-3). In order to place the natural frequencies of the box much higher than the air resonance frequencies the walls of the resonance box are chosen from thick 7-mm plywoods and 5-mm cardboards. Sound-holes geometries to be studied are carved in a plywood with thickness 3 mm and are placed on the top plate (Fig. A-4). Use of advanced laser-cutting technologies enabled us to carve complex sound-hole geometries such as the lute rosettes. All the laser cutting process has been done in Media lab and the workshops of the Architecture department at MIT.

The cavity mode is excited with a speaker (Digital BA735, Boston Acoustics Inc.), placed in the distance of 20 cm from the sound-hole, and the receiver was chosen as a microphone (Olympus ME-15) placed inside the resonance box. The microphone is placed on the back plate inside the resonance box to reduce the ambient noise. Moving the microphone to different locations on the back plate showed no significant change in the measurements as is expected because of the small size of the resonance box (30 cm) compared to the wavelength (150 cm). The speaker distance from the resonance box has been changed from 10 cm to 100 cm. Different orientations of the speaker have also been tried by changing the angle between the speaker and resonance box top plates up to 30 degrees. The change in distance and orientation

of the speaker showed no significant change in the measurements. For distances over 100 cm a reduction in signal to noise ratio has been observed. The input signal was designed as a slowly varying ramp around the resonance frequency of the specific opening. The microphone outputs were analyzed by a computer-based acquisition system. The measurements were made in the time domains, then a Fourier transform was used to obtain the frequency domain spectra. The Fourier spectra were window-averaged with a window width of 1000 samples (The sample frequency of the system is 20000 Hz). The resonance frequency is measured as the mean of the two frequencies at which 3-dB down line cuts the curve, that is  $f_0 = (f_1 + f_2)/2$  (Fig. A-5). This method gives a low standard deviation for the peak of the curves symmetric around the resonance peak as is in our case. The tests had been first run in closed spaces where distorted resonance curve (as minor second or third peak) had been observed due the reflection from the walls. In order to eliminate the effect of the room on the resonance patterns [6], all the tests have been run in open area (in Killian court at MIT) where the closest wall is at least 50 m far from the setup (the wavelengths we worked with were below 1 m, which are much less than 50 m, the characteristic length of the open area). The resonance curves we measured in the open area were consequently clean of any distortion because of the long distance of the walls as reflectors from the setup.

To quantify the damping effects, the 3-dB and 10-dB down bandwidth of the pressure squared curve normalized to peak are measured directly from the spectrum (Fig. A-5). The 3-dB bandwidth measurements have been cross validated by another method [21], which measures the amplitude decay of the output when the sound-hole is exposed to tone bursts at the resonance frequencies. After exciting the Helmholtz resonator and then removing the excitation source, the system can be modeled as a free simple damped oscillator ([13]). The pressure inside the box can then be expressed as [13],

$$P(t) = P_0 e^{-\zeta 2\pi f_0 t} \sin(\sqrt{1 - \zeta^2} 2\pi t + \phi) \quad (3.1)$$

where  $P_0$  is the pressure amplitude,  $\zeta$  the damping factor,  $f_0$  the resonance frequency and  $\phi$  is a phase angle. The following relation holds between the damping factor  $\zeta$  and the 3-dB bandwidth  $\Delta f$  [19]:

$$\Delta f = 2\zeta f \quad (3.2)$$

So, by measuring the rate of the decay of the pressure oscillation inside the box, we can find a different way to calculate the 3-dB bandwidth  $\Delta f$ . The rate of the decay is obtained by measuring the slope of the decay of  $\ln(P(t)/P_0)$  as a function of time (see Fig. A-6) where  $P_0 = 1$  is a reference pressure. The slope of the decay is independent of the reference pressure  $P_0$ . From Eq. 3.1, this slope is given by the coefficient of  $t$  in the exponential term,

$$\alpha = -\zeta 2\pi f_0 \quad (3.3)$$

From Eqs. 3.3 and 3.2 the 3-dB bandwidth,  $\Delta f$  is given by,

$$\Delta f = -\frac{\alpha}{\pi} \quad (3.4)$$

One of the parameters for calculating the air resonance frequency is the cavity volume, which is difficult to measure in instruments with complex sound box such as violin. The cavity volume of the members of the violin family was measured by assuming top and back plates to be flat. By taking picture of each instrument individually at Johnson String Instrument and inserting the picture in AutoCAD software, we measured the area of the top and back plate and the height of the sound box as shown in Fig. A-7. So, the volume of cavity can be found as the product of the obtained area and the height by neglecting the 3D curvature of the top and back plates at this stage. To include the volume change due to 3D curvature of the top and back plate, a correction factor was calculated for a full length violin by filling the instrument with sand and measuring the exact cavity volume (Fig. A-8). The volume of the cavity by flat top and back plates should be multiplied by 1.145 to give the real volume. Due to lack of access to other instruments in the violin family for

the destructive volume measurement by sand, this correction factor has been used for other instruments.

# Chapter 4

## Lute Rosette

The resonance due to Lute rosettes, considered as one of the most complex sound-holes, has been characterized theoretically and empirically using the method developed. Lute rosettes come in variety of shapes from which we investigated the following traditional roses: Wendelio Venere 1592 (Fig. A-9 a), Warwick Hans Frei 1540 (Fig. A-9 b and e), in Padov 1595 (Fig. A-9 c), Sebastian Schelle 1744 (Fig. A-9 d) and Wendelin Tieffenbrucker 1590 (Fig. A-9 f) [1]. The percentage void area of the above rosettes are 44%, 43%, 35%, 36%, 31% and 45%, respectively. The circular sound-hole theory for air resonance frequencies, which is based on the void area, predicts the air resonance frequency to change more than three semi-tones from Warwick Hans Frei rosette with 31% void to Wendelin Tieffenbrucker rosette with 45% void. The resonance frequency in this theory is obtained by the following expression,

$$f_0 = \frac{c_0}{2\pi} \sqrt{\frac{A}{Vh}} \quad (4.1)$$

where  $A$  is the total void area,  $h$  the wood thickness,  $V$  the cavity volume and  $c_0$  is the sound speed. This formula works well for opening with neck length (here the wood thickness) much greater than the opening diameter. For small opening neck length, the above formula gives considerable error, which is corrected by replacing  $h$  with effective thickness  $h_e$ . The effective thickness can only be obtained analytically for circular and elliptical openings, which is equal to  $h_e = h + \pi R/2$  for a circular

opening with radius  $R$ .

In contrast to the three semi-tone variation by previous methods, the variation in air resonance frequencies of the above rosettes was observed to remain within 32 cents (each cent is one percent of a semi-tone) by our rigorous approach, with the Hans Frei I (Fig. A-9 b) having the highest and the in Padov (Fig. A-9 c) having the lowest resonance frequency. Hence, we concluded that the resonance frequency of the lute rosettes has low dependency on the total void area of the rose pattern, which is also in contrast with the general impression among some lute players. For better understanding of the dependence of resonance frequency on hole density, a lower and upper limit is found for the rosettes mentioned above. The resonance frequencies of different lute rosettes are compared to the resonance frequencies of radial and angular distributions of the void area. In the radial distribution (Fig. A-10 (a)), the void area is distributed between nine rings with the diameter of the outer ring equal as the outer diameter of lute rosettes. The width of each rings varies equally from zero to its maximum value where the void covers the whole area. In the angular distribution (Fig. A-10 (a)), the void area is distributed between angular sectors where the outer diameter is again equal to the outer diameter of the lute rosettes. The sectors' angle varies equally from zero to their maximum value where the whole area is covered by void. The holes with angular distribution proved to be the lower limit and the holes with radial distribution proved to be the upper limit for the resonance frequencies of the above lute rosettes (Fig. A-11).

In a systematic analysis of a circular opening with diameter  $d_o$ , blocked with an inner circle of diameter  $d_i$ , we showed that the resonance frequency of the resonators has low dependency to the central blockage (Fig. A-12). We observed that the resonance frequency changes less than a semi-tone while the central area of the opening is blocked by 50 percent, i.e.  $d_i/d_o = 0.7$  (Fig. A-12). When the inner diameter exceeds 80 percent of the outer diameter ( $d_i/d_o > 0.8$ ), a steep drop in the resonance frequency is observed. This theoretical analysis, validated closely by experiments, suggests that the outer rim of circular openings has major effects on the resonance frequency. This fact implies that the wood inside the circular sound-holes might be saved without

significant changes in Helmholtz resonance frequency of the instrument. In the case of the lute rosettes, the central part is filled with patterns that add to the wood area of the soundboard, as well as the aesthetics of the instruments [24].

In an experimental damping analysis, we showed that the 3 dB-down bandwidths of the air resonance curves for the rosettes shown in Fig. 1 vary within 10 percent of a semitone. The bandwidth of the air resonance curve is due to radiation damping and viscous damping. The radiation damping is a direct function of the conductance of the opening, or in another words, a direct function of the resonance frequency [7, 13]. Since the resonance frequencies for different patterns varies negligibly, the variation in radiation damping is also small. The viscous damping is a function of the wall area over which the majority of the air flux passes. According to the flux distribution over a rosette (Fig. A-13), the majority of the flux passes by the outer edge of the opening. As a result, for rosettes with the same outer diameters the effect of viscous damping does not differ significantly among different patterns. So, the variation of both the radiation and viscous damping would be small, which is consistent with the experimental results.

The air flow distribution over the lute rosettes, obtained theoretically via the developed method, confirms that the major flow passes through the outer edge of the opening. For the case of the Tieffenbrucker rosette (Fig. A-13), 50 percent of the flux passes through a rim enclosed between the outer boundary of the opening with radius  $r_0$  and a circle with radius  $0.84r_0$ . The air flow distribution explains the slight changes of resonance frequency (less than a 32 cents) among different rosettes studied, compared to the changes in void areas (more than 45 percent). As a general trend, the flow speed tends to be higher near the edges, which can be observed even in the small holes in the middle of the pattern. The overall flow through each individual hole tends to be higher if the hole is closer to the outer boundary of the opening.

The rosettes in lute, as well as the ones in theorbo, also serves to cover the bracings structure underneath, which would aesthetically be displeasing. This barring structure helps to transfer modal energy across what would otherwise be a void in the overall soundboard structure of the instrument. The mentioned bracing structure is much

sparser than the rosette and so has negligible effect on the resonance frequency.

The air resonance frequency of Andreas Berr lute has been measured by using the same experimental approach. The test has been carried out at the Museum of Fine Arts in Boston where the instrument is kept. The instrument made by Andreas Berr (Austrian, 1656-1722) is 81 cm in length, 28.3 cm in width and 13.5 cm in depth. The rose diameter was measured as 59 mm (a replicate of the rose is shown in Fig. A-14). The materials used are Ivory, spruce and ebony. The spectrum of the instrument at low frequencies showed an air resonance frequency at 124 Hz Fig. A-15. Because of the complex geometry of the sound box, the volume measurement has not been done.



# Chapter 5

## Violin f-hole

Violin sound-holes have been evolved over the course of centuries to the present-day f-hole geometry. We showed that acoustic effects, including the economy of the void and the increase in the bandwidth of the air resonance curve, are the potential driving forces in this evolution process. In violin family, the circular openings in 10th-century viols [8] has gone through gradual changes to semi-circular opening in Lyras in 13th century [8], crescent-shape [16] and semi-circular strip [20] openings in 13th century, primary c-hole [20] and c-hole in early viols and violin of 16th century [5] and eventually to the present-day f-holes stayed unchanged since 17th century [5]. We carved openings with the above geometries with sizes that make the resonance frequencies of all the patterns equal. This size for each opening was obtained theoretically by the developed approach to measure the resonance frequency of general openings. The resonance curve of each pattern has been measured experimentally and the 10-dB bandwidth, defined as the width of the resonance curve at 10-dB down the peak, has been measured. The 10-dB down bandwidth was chosen since the air resonance peak in violin stands above the background trend by roughly 10-dB (Fig. A-17). We observed the increase in the bandwidth of the air resonance curve and the decrease in the void area as two significant trends in the mentioned evolutionary process (Fig. A-16).

Comparing the circular opening to the f-hole with a given resonance frequency, we observed an increase of a semi-tone in the 10-dB-down bandwidth of the resonance curve, and a saving of the missing wood by a factor of more than two (Fig. A-16). The

air resonance peak in violin spectrum [2] shows that the 10-dB down bandwidth is more appropriate than the more standard 3-dB down bandwidth (Fig. A-17) because the 10-dB bandwidth is the width of the peak that is added to the spectrum compared to the nearby trend without the peak. The increase in bandwidth of f-hole can be attributed to the high air velocity at the necks of the f-hole (Fig. A-21). The high rate of flow at the necks increases the viscous damping substantially. The tendency in bandwidth increase has the following potential bases: (i) error reduction in placing the air resonance for design purposes, (ii) shortening of resonance duration and making the instrument spectrum even by lowering the peak of the air resonance frequency, which helps remove wolf notes and (iii) amplifying a wider range of frequencies. The trend in evolving to a more stretched shape can be attributed to the tendency in having parity with the geometry of the violin body. The more efficient sound-holes in void economy, such as f-hole, have the benefit of less interference with the primary mode shapes of the soundboard. Additionally, a soundboard with less missing wood have less vertical fibers cut, which is beneficial in preserving the longitudinal strength of the wood.

Previously, the air resonance frequency of violin is obtained by the following two approaches. In the first approach, f-hole geometry is approximated by ellipse and circles [6, 18, 10]. This approach is based on a network description of the air and top plate resonances [18]. In this approach the inertance of f-hole is estimated by reducing it to an ellipse matching to the sinuate slot and two circular holes matching the ends. The initial parameters of the network include the inertance of each hole and the capacitance of volume. The inertance of each hole itself is composed of internal and external inertances describing the lower and upper parts of the f-hole, which are in contact with the air in the body and outside the body, correspondingly. The contribution of the internal and external inertance is assumed to be not equal and a parameter is attributed to account for the ratio between them. By comparing the resonance frequency from this network to the experimental results, the initial parameters are adjusted. The change in parameters varied from zero percent to 33 percent [18]. In the second approach, the following equation is used to obtain the

resonance frequency [4]:

$$f = \frac{c_0}{2\pi} \sqrt{\frac{A}{(h + a\sqrt{A})V}} \quad (5.1)$$

where  $A$  is the total void area,  $c_0$  the sound speed,  $V$  the volume of the resonance box,  $h$  the thickness of the board and  $a$  is adjusted empirically to agree with experimental results [4], which depends on the shape of the opening. Both of these approaches have the drawback of being case dependent, that is by changing the instrument the empirically determined coefficient has to be determined again. In addition, this approach results in a different functionality of the resonance frequency on the void area from the one obtained via the general sound-hole theory discussed below.

Plugging Eq. 2.3 into Eq. 2.2, we have the following relation for the air resonance of general opening,

$$f = \frac{c_0}{2\pi} \sqrt{\frac{A}{(h + A/C)V}} \quad (5.2)$$

where  $C$  is the conductance of the f-hole with zero wood thickness. Comparing Eqs. 5.1 and 5.2, we see the difference in the functionality of the void area  $A$  between the semi-empirical method used and our rigorous approach for general sound-hole. We applied our approach developed for general sound-holes to violins with f-hole geometry traced from a drawing of the Emiliani Stradivari of 1703 (The photograph of this violin is shown in Fig. A-18 [5]). Using the geometry of Emiliani Stradivari of 1703 for a pair of f-holes with unit vertical length, we obtained the conductance of an infinitely thin opening with the same geometry as  $C = 1.01$  (unit length) and the void area as  $A = 0.192$  (unit length squared). Using Eq. 2.3, and scaling the vertical length from the unit length to  $L$ , we have,

$$f = \frac{c_0}{2\pi} \sqrt{\frac{L(0.193)}{V(0.192 + 1.01h/L)}} \quad (5.3)$$

where  $L$  is the vertical length of the f-hole. Use of Eq. 5.3 is valid for all the members of the violin family as long as the f-hole geometry remains the same as the Stradivari

of 1703. For violins with different f-hole geometry similar expression as Eq. 5.3 can be obtained. The theoretical results obtained from Eq. 5.3 show a close agreement to the experimental results (Fig. A-19), while using Eq. 5.1 results in a considerable offset for each instrument that is usually corrected empirically for the corresponding instrument [4]. To compare the air resonance frequencies of violin family obtained by Eq. 5.1 and Eq. 5.3, we defined the following error function,

$$error = \sqrt{\sum_{i=1}^N (f_i - f_{e,i})^2 / N} \quad (5.4)$$

where the resonance frequency  $f_i$  is the air resonance frequency of the  $i$ -th instrument obtained either by Eq. 5.1 or 5.3 and  $f_{e,i}$  is the the resonance frequency of the corresponding instrument obtained experimentally.  $N$  is number of instrument studied in the family. The lower the error defined above, the better a formulation describes the air resonance frequencies of the members of the violin family. The error between the experimental frequencies and the ones obtained by Eq. 5.3 is obtained as 5.06 Hz. To obtain the error between the experimental frequencies and the ones obtained by Eq. 5.1, first we should adjust the parameter  $a$ . We chose different members of the violin family to find  $a$ , and then compare the experimental frequencies with the one obtained from Eq. 5.1 using the same  $a$ . Based on which instrument to choose for adjusting  $a$  the error would be different. The error of using Eq. 5.1 is shown in Table B.1. The instruments shown in the table are the one that used for adjusting the parameter  $a$ . The same value of  $a$  is then used for other instruments. As it can be seen, a drawback of using Eq. 5.1 is that the error changes based on the instrument chose to adjust the parameter  $a$ . In addition, the error of using Eq. 5.1 is always more than the error of our approach given as 5.06 Hz.

In a systematic analysis we have also investigated the effect of changing the distance between the f-holes on air resonance frequency (Fig. A-20). According to our result, by changing the distance the resonance frequency varies, implying the interaction between the two f-holes. Nevertheless, the frequency variation due to f-hole spacing is not significant. As is shown in Fig. A-20, if the distance between f-holes is

changed by a factor of two, the variation in resonance frequency would be less than a semi-tone. As it can be seen from Fig. A-20, variation within 5 percent in distance between the f-holes results in variation of less than 5 cents.

In order to investigate the effect of the geometry of the f-hole on air resonance frequency, the flux distribution over the opening is studied (Fig. A-21). The flux is more concentrated at the neck of the f-hole (the location where the circular parts are connected to the sinuate part), where the opening is more constricted. The high rate of air displacement at the neck makes the damping sensitive to the shape of the neck region. So, variation in the geometry of the neck results in variation in bandwidth of the resonance curve. A comparison of an f-hole opening with a circular opening with the same resonance frequency, shows 64 percent increase in bandwidth. The substantial increase in the bandwidth can be attributed to the increase in viscous damping due to irregular shape of f-hole, since the radiation damping is only a function of the conductance, which is the same openings with the same resonance frequency.



## Chapter 6

### Multiple Sound-holes

The sound-hole in instruments such as theorbo and oud appears in the form of three circular holes. It might be expected that the main air resonance frequency can be approximated by the linear superposition of the effect of each hole as has been done in violin family [18]. In this approximation, the conductance of each hole, for which the analytical expression exists, is superimposed to each other to obtain the conductance of the whole opening. Using the developed method to obtain the air resonance frequencies in theorbo and oud, we have shown that the linear superposition approximation leads to significant error (Fig. A-22). For oud, in which two of the holes are much smaller than the other, the linear superposition leads to overestimation of more than two semitones in air resonance frequency (Fig. A-22). For theorbo, in which the holes are in comparable size and closer to each other, the error due to superposition appears to be more than four semitones more than the actual value (Fig. A-22).

The error in superposition approximation stems from the assumption that each hole acts independently at resonance. In contrast, the flow passing through each hole interacts with each other that makes it essential to solve the flow field simultaneously for the whole opening (Fig. A-23). As the distance between the holes increases, the amount of the interaction decreases and the superposition method gives a better approximation. This fact explains the higher error in theorbo in which the holes are closer to each other compared to the one in the oud (Fig. A-22). It should be mentioned that the use of the developed method is valid for multiple openings as long

as the distance between the holes ( $\sim 5$  cm in theorbos and  $\sim 20$  cm in ouds) is much less than the wavelengths at resonance ( $\sim 2$  m).



# Chapter 7

## Conclusion

We developed a general method that enables us to calculate the air resonance frequencies of instruments with complex sound-holes such as the one in violin, lute and oud families. In addition, using this method we are able to analyze the flow transport distribution over general openings. Using this method, we presented the potential physical principles behind the geometrical design of complex sound-holes.

We showed that the majority of the air flow passes through the near-the-edge area of the circular opening, and consequently, the central part of such sound-holes contribute least to the air resonance. This theoretical analysis, confirmed closely by experiments, suggests that the outer rim of circular openings has major effect on the resonance frequency. An important consequence of this finding is that the resonance frequency is not necessarily proportional to the square root of the void area. In fact we showed that if the aspect ratio of the sound-hole geometry is fixed, the resonance frequency is proportional to the fourth root of the area. The fact that the majority of the air transport happens at the outer rim implies that the wood inside the sound-hole can be used more efficiently, which might have been the cause to the emergence of the rosette lutes. Using the developed method, it was observed that variation in air resonance frequencies of the rosettes studied (we studied seven different rosettes with fixed outer diameters) varies within 32 cents. The air flow distribution over the lute rosettes, obtained theoretically via the developed method, confirms that the major flow passes through the outer edge of the opening.

Violin sound-holes have been evolved from circular geometry to the present-day f-hole over the course of centuries. We showed that the acoustic effects, including the economy of the void and the increase in the bandwidth of the air resonance curve, are the potential driving forces in this evolution process. In violin family, the circular openings in 10th-century viols has gone through gradual changes to semi-circular opening in Lyras in 13th century, crescent-shape and semi-circular strip openings in 13th century, primary c-hole and c-hole in early viols and violin of 16th century [5] and eventually to the present-day f-holes stayed unchanged since 17th century [5]. Comparing the circular opening to the f-hole with a given resonance frequency, we observed an increase of a semi-tone in the 10-dB-down bandwidth of the resonance curve, and a saving of the missing wood by a factor of more than two. The 10-dB bandwidth was chosen because the peak of the air resonance in violin stands roughly 10-dB above the background trend. Additionally, a theoretical expression for the main air resonance frequencies of violin family has been obtained using the developed method. This new expression implies that for thin soundboard compared to the f-hole length, the resonance frequency is proportional to the square root of the f-hole length. Consequently, the resonance frequency is proportional to the fourth root of the f-hole area, provided that the aspect ratio remains fixed. This theoretical expression show a close agreement to the experimental results, while the approach based on circular sound-hole theory results in a considerable offset that is usually corrected empirically.

The sound-hole in instruments such as theorbo and oud appears in the form of three circular holes. Using the developed method to obtain the air resonance frequencies in theorbo and oud, we have shown that the linear superposition approximation leads to significant error. For oud, in which two of the holes are much smaller than the other, the error due to linear superposition is more than two semitones. For theorbo, in which the holes are in comparable size and closer to each other, the error due to superposition appears to be more than four semitones.

# Appendix A

## Figures

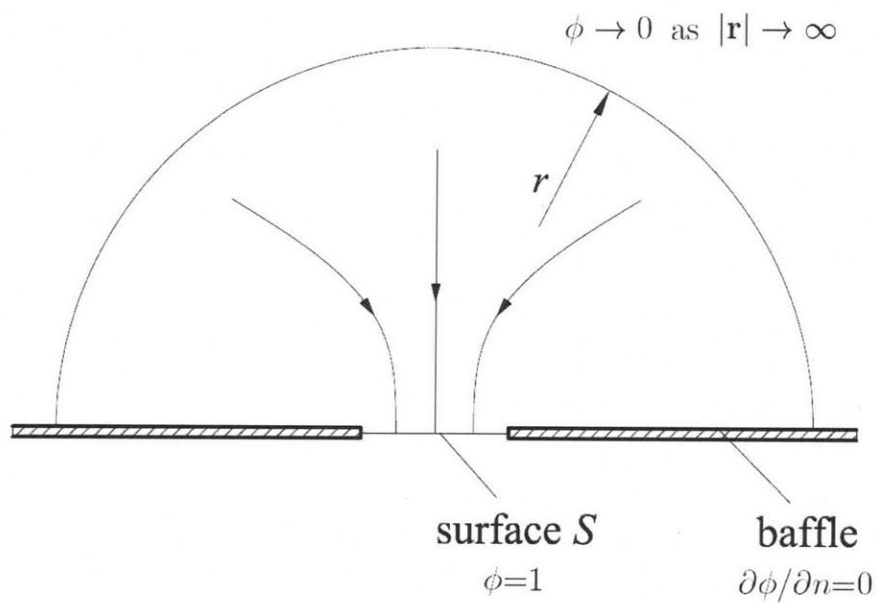


Figure A-1: Schematic of an opening. The potential  $\phi = 0$  on the opening surface,  $\partial\phi/\partial n = 0$  on the baffle and  $\phi \rightarrow 0$  as the distance from the center of the opening  $|\mathbf{r}| \rightarrow \infty$ .

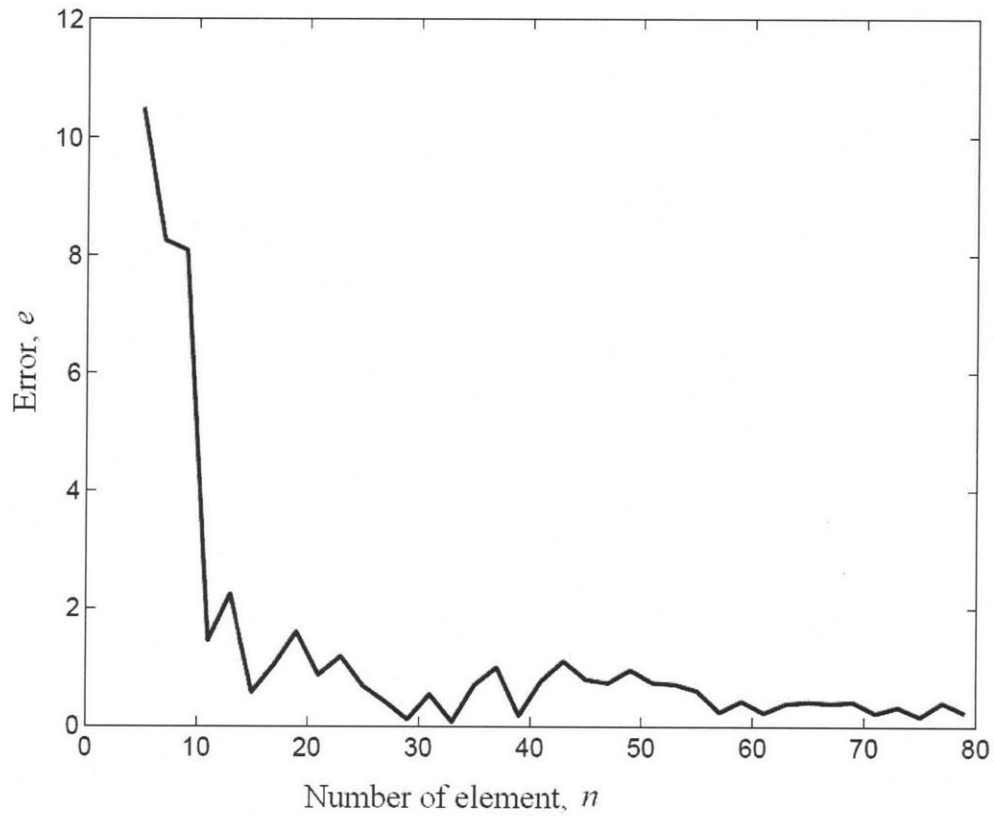


Figure A-2: The error in validation of the numerical scheme for calculating the conductance of a circular opening. The error percentage, calculated as  $e = (C_{numerical} - C_{analytical})/C_{analytical} \times 100$  is shown versus  $n$  the number of element on each side (i.e., the pattern is digitized as  $n \times n$  grid and the total number of elements is  $N = n^2$ ).

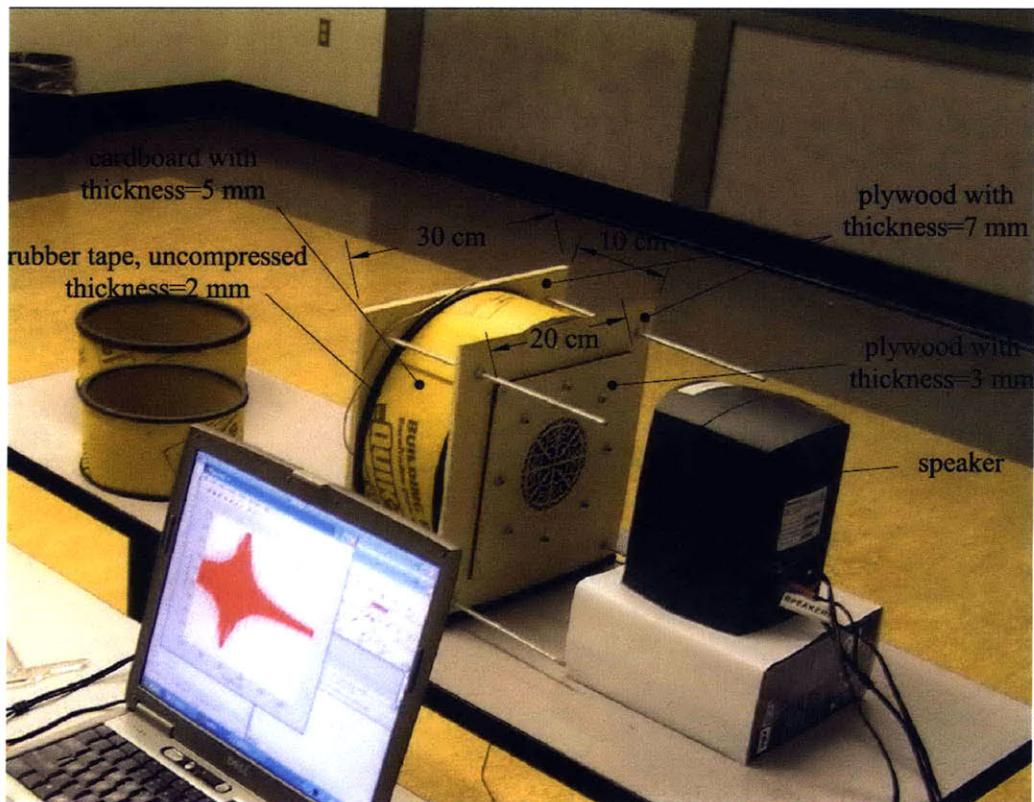


Figure A-3: Resonator setup is shown. The resonance box is made of a cardboard with thickness of 5 mm, and top and back plates out of plywood with thickness of 7 mm. The pattern is carved on a 3-mm plywood and mounted on the top plate. The contact between the top and back plates and the cardboard are sealed with rubber tapes. The microphone as the receiver is placed inside the resonance box attached to the back plate. The speaker is placed in front of the pattern.

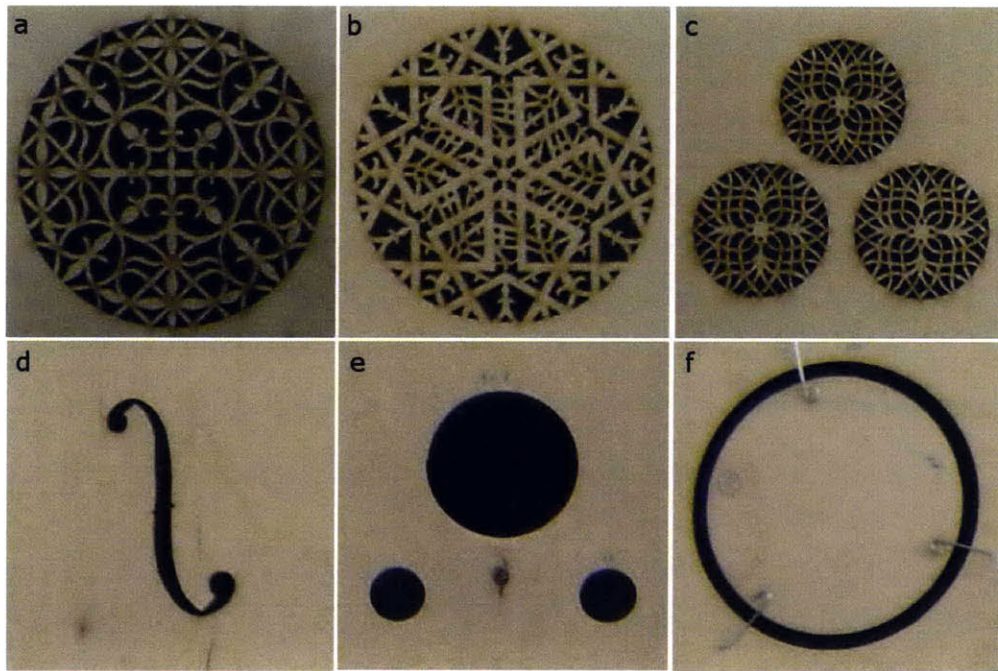


Figure A-4: Opening patterns: (a) Lute rose (Wendelin Tiffenbrucker [1]), (b) Lute rose (Warwick Hans Frei [1]), (c) Theorbo rose [1], (d) Violin f-hole, (e) Oud rose (pattern removed) and (f) sound-hole in the form of a ring.

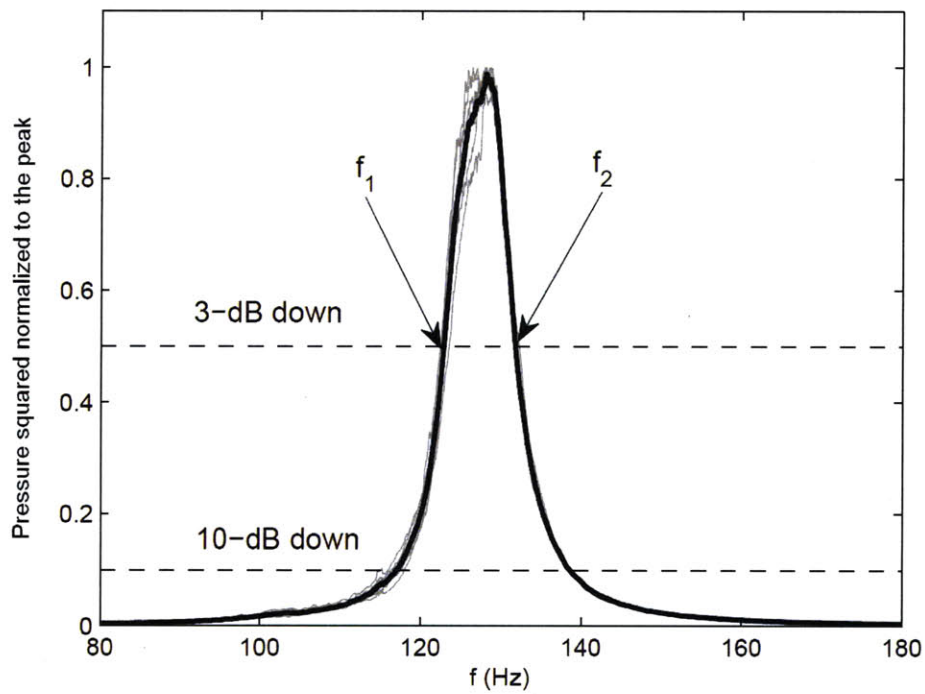


Figure A-5: Air resonance curves of f-hole are shown for  $n = 9$  measurements (gray curves). The sound level is normalized by the peak level. Each curve is smoothed by window averaging with window width of 1000 samples. The black line represents the average of the nine measurements. The horizontal dotted line represents the 3-dB and 10-dB down level from the peak. Frequencies  $f_1$  and  $f_2$  are where the 3-dB down level cuts the curve. The peak frequency is then obtained as  $f_0 = (f_1 + f_2)/2$ .



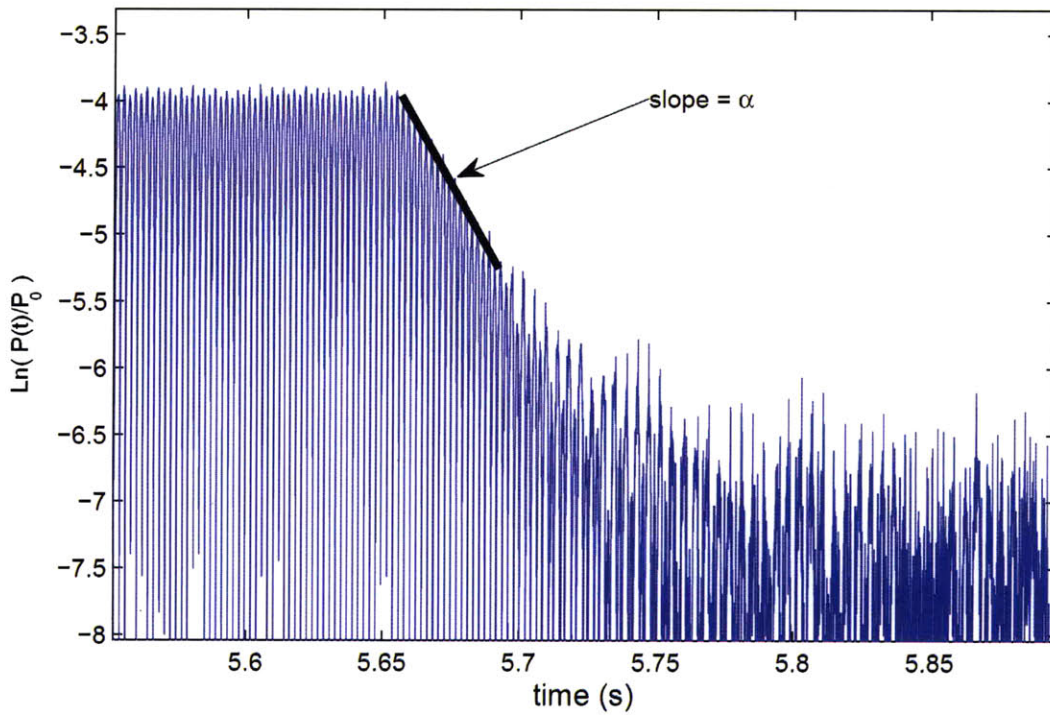


Figure A-6: Measuring the decay slope of the amplitude of the pressure inside the box provides a different method to calculate the 3-dB down bandwidth of the resonance curve shown in Fig. A-5. The slope  $\alpha$  is measured during the free oscillation of the resonator after the excitation source is removed (in this figure, after 5.65 s). The 3-dB down bandwidth  $\Delta f$  is then obtained as  $\Delta f = -\frac{\alpha}{\pi}$ . The reference pressure  $P_0$  is set to  $P_0 = 1$ . The slope  $\alpha$  is independent of the value of  $P_0$ .

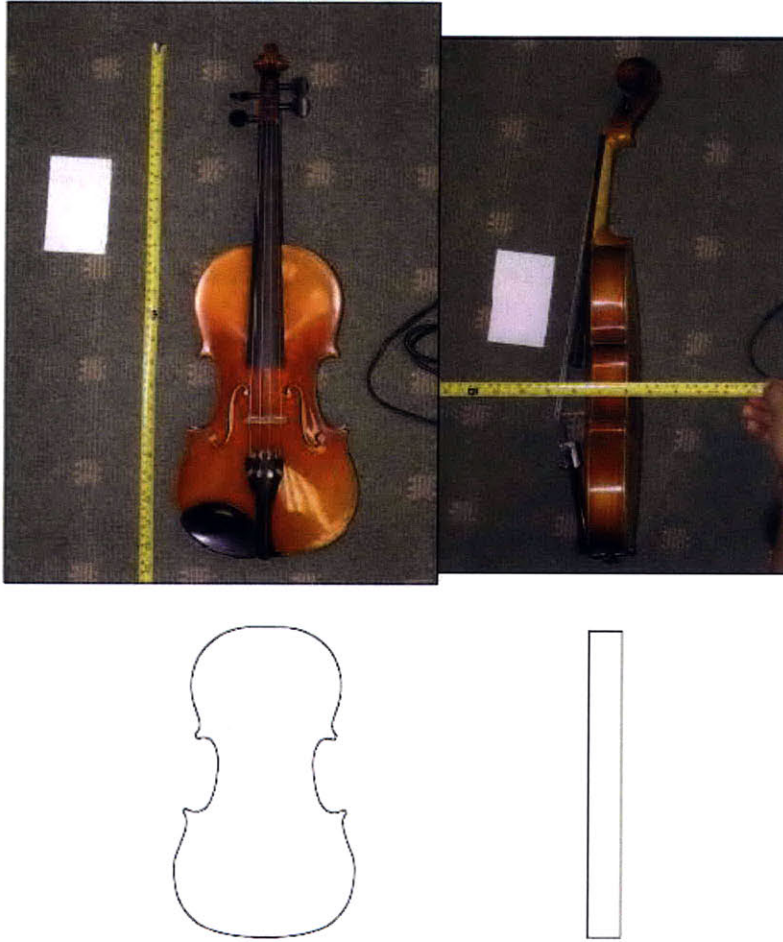


Figure A-7: The volume of the sound box is measured by first assuming the top and back plates to be flat and then correct this assumption by a correction factor obtained by filling the volume with sand. The flat area of the top and back plate and the height of the box is measured in AutoCAD by inserting the images of each instruments.



Figure A-8: The cavity volume is measured by filling the violin with sand.

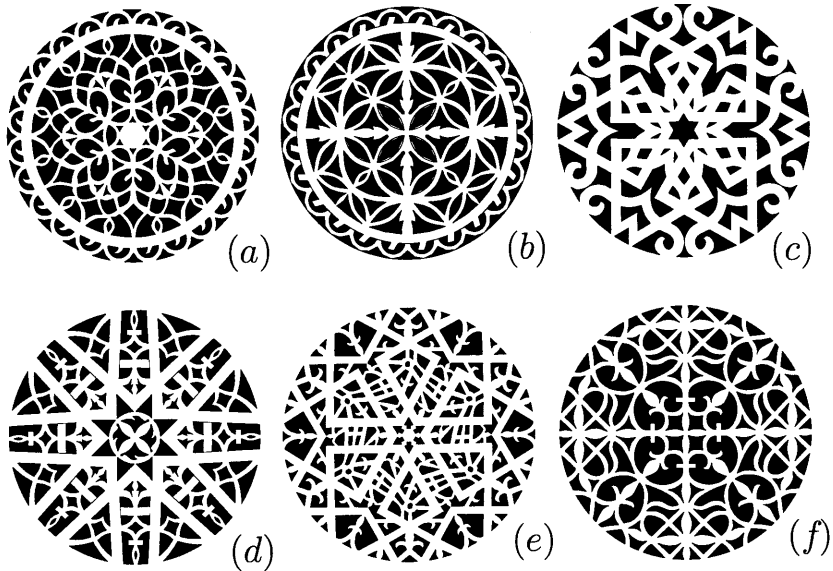
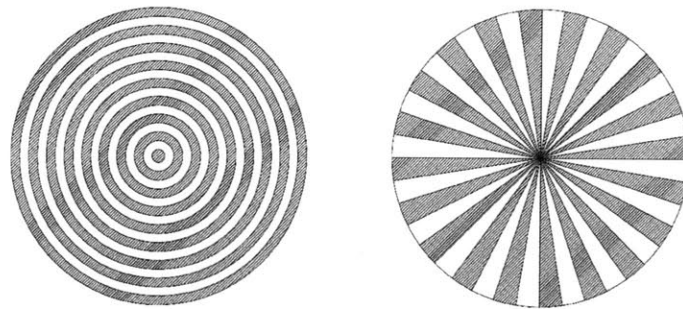


Figure A-9: The air resonance of the following lute rosettes is characterized: (a) Wendelio Venere 1592 (b) Hans Frei 1 1540 (c) in Padov 1595 (d) Sebastian Schelle 1744 (e) Hans Frei 2 1540 (f) Wendelin Tieffenbrucker 1590. Comparing the resonance frequency due to each rosettes, we observed a variation within 30 percent of a semitone. With center frequency of 123 Hz used in the experiment, the 3-dB-down bandwidth variation stays within eight percent of a semi-tone. It should be mentioned that the outer diameters and thicknesses of all the rosettes and the experimental setup such as the box volume, microphone and speaker placements were the same in the above comparison.



(a) radial distribution

(b) angular distribution

Figure A-10: (a) The radial distribution of the void area, (b) the angular distribution of the void area used as the lower and upper limits for the resonance frequencies of the discussed lute rosettes (Fig. A-11). The radial distribution is composed of nine rings with equal widths. To increase the void area, the width of each ring is equally increased. The angular distribution is composed of 20 sectors with equal angles. To increase the void area, the angle of each sector is increased equally.

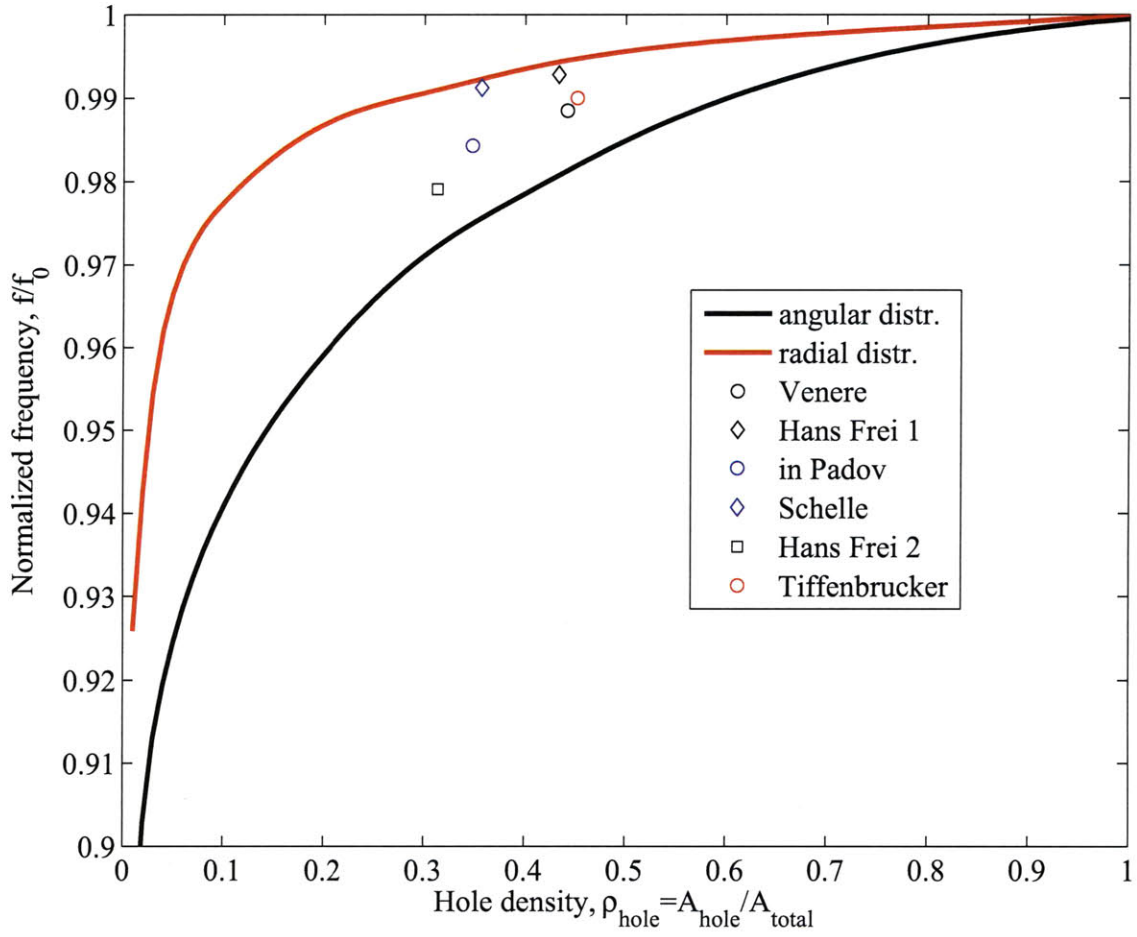


Figure A-11: Comparing the resonance frequencies of different lute rosettes to radial and angular hole distributions (Fig. A-10). The frequency  $f_0$  and the area  $A_{total}$  represent respectively the resonance frequency and the area of a circular opening with the same diameter of the outer diameter of lute rosettes studied.

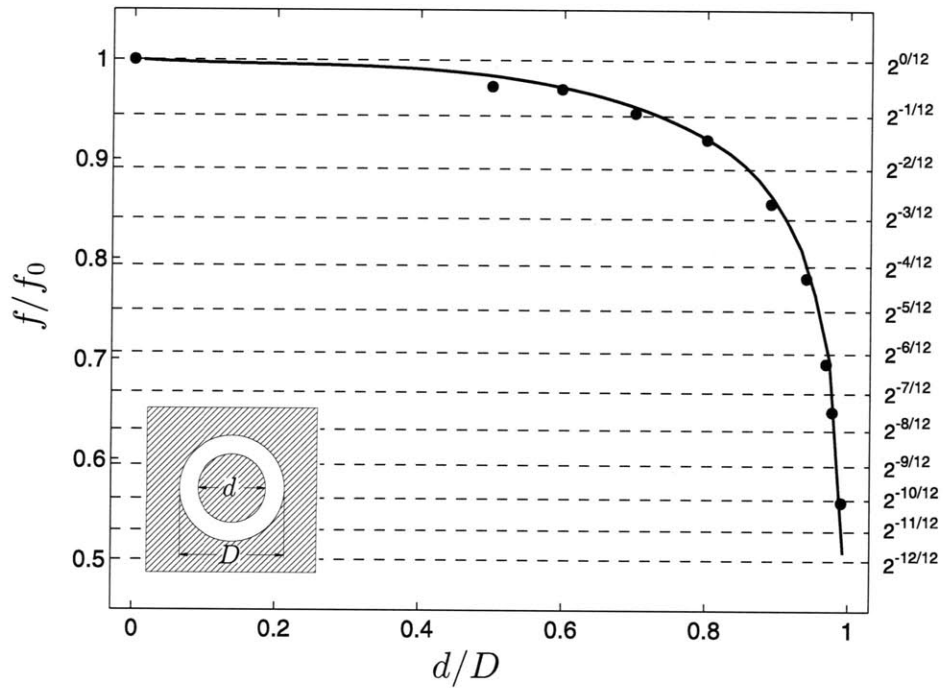


Figure A-12: Resonance frequency of a ring with different ratio between the outer and inner diameters is shown. The diameter of the inner and outer circles are shown by  $d$  and  $D$ , respectively. The frequency  $f_0$  corresponds to the resonance frequency of an opening with diameter  $D$  ( $d=0$ ). The vertical axis on the right are scaled on semitones (In diatonic system, each octave is divided into 12 equidistant intervals called semitone. So, each semitone is  $2^{1/12}$  of an octave). The results show that the resonance frequency is highly dependent on the outer periphery of the opening.

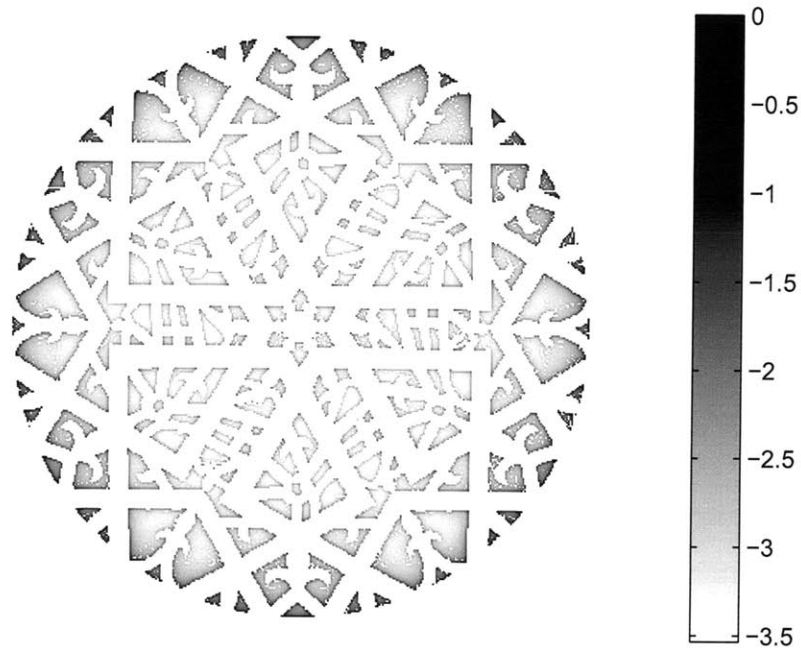


Figure A-13: Flux distribution profile in log scale,  $\log(\sigma)$  (the source strength  $\sigma$  is obtained from Eq. 2.9) is shown for Warwick Hans Frei lute. The flux is normalized by its maximum value, so the zero value in the colorbar represents the maximum flux value.



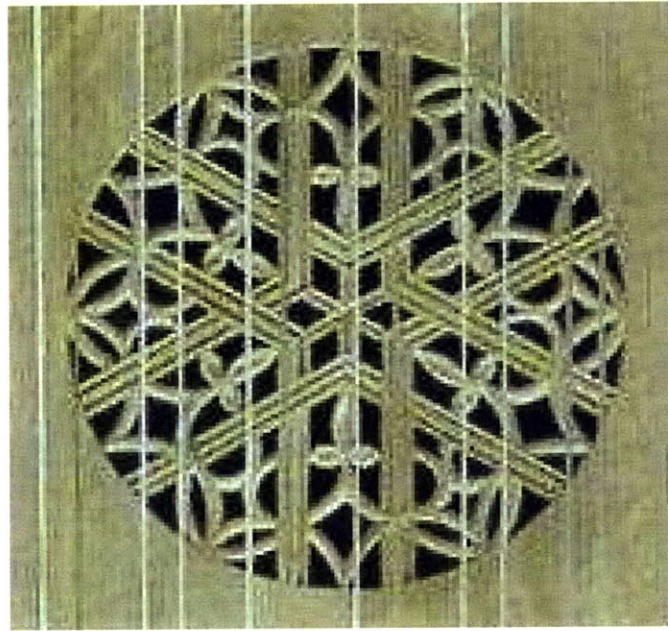


Figure A-14: The rosette on Andreas Berr lute. The image is taken from the website of Stephen Barber and Sandi Harris, lute makers [1].

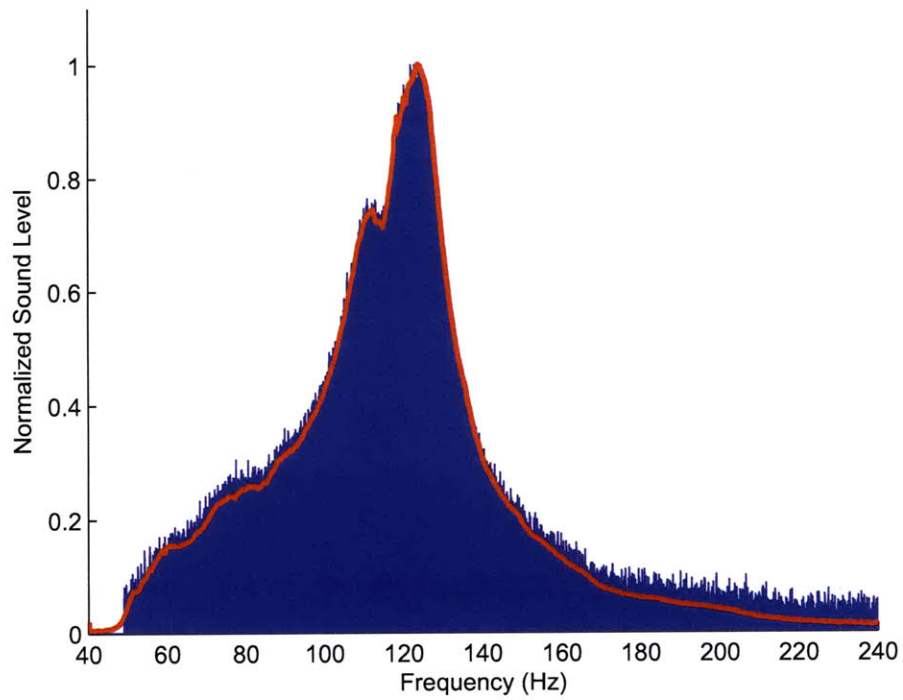


Figure A-15: The spectrum of the Andreas Berr lute at low frequencies. The sound level is normalized by the peak level. The air resonance frequency corresponding the peak shown was measured at 124 Hz. The blue curve shows the raw data, and the red line shows the process data after taking Fourier Transform. The asymmetry of the resonance curve is due to the reflection of sound from the walls.

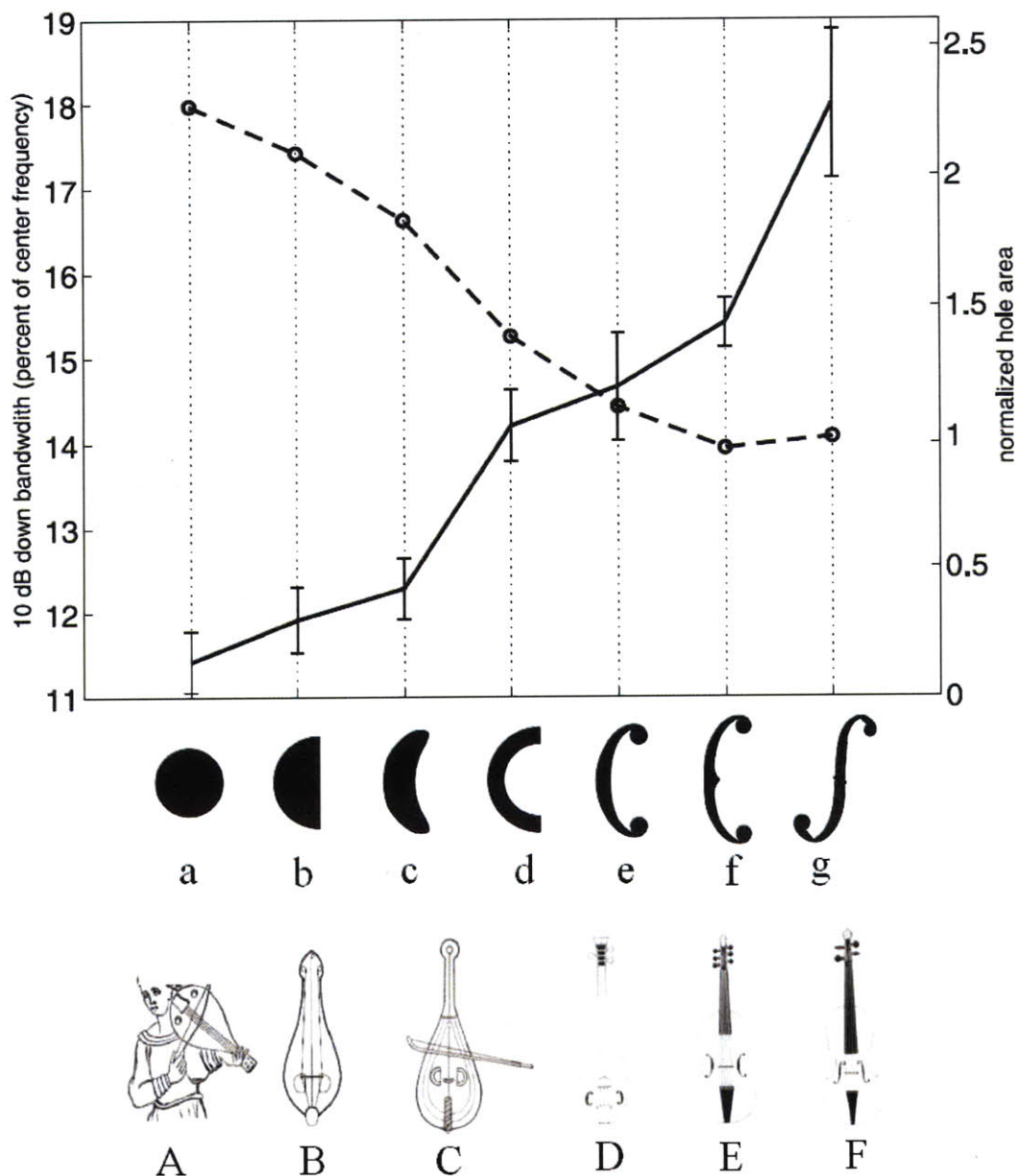
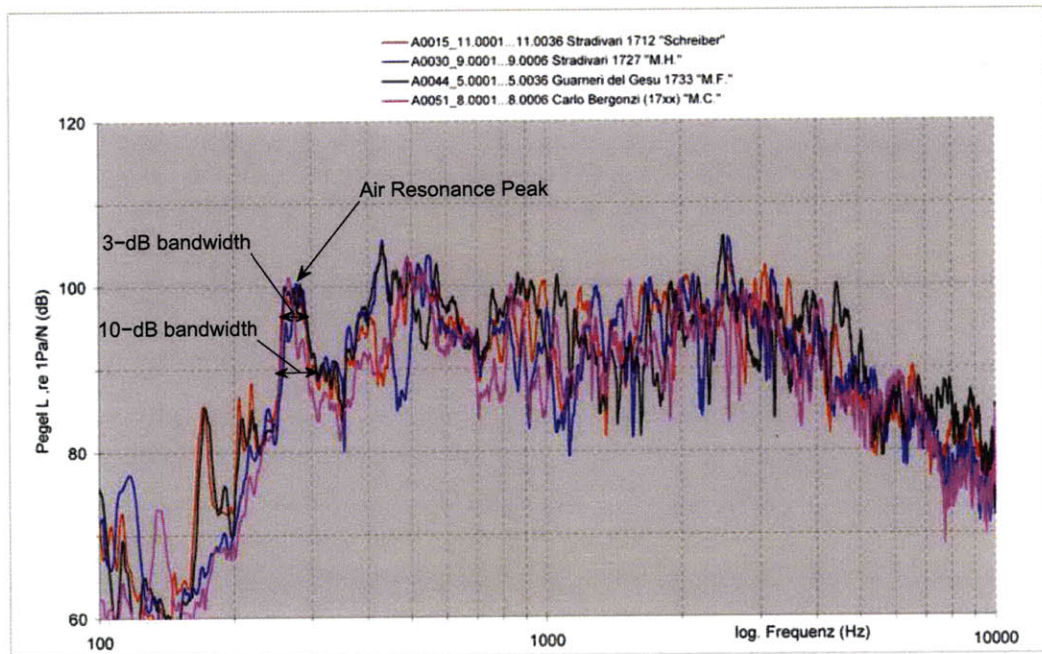


Figure A-16: The line of development of sound-holes in violin is shown for circular opening (a) in 10th-century viols [8] (A), semi-circular opening (b) in Lyras in 13th century [8] (B), crescent (c) [16] and semi-circular strip (d) [20] in 13th century instruments (C), primary c-hole (e) [20] [20] and c-hole (f) in early viols and violins (D,E) in 16th century [5] and present-day f-hole (g) in violins (F) staying unchanged since 17th century [5]. The 10-dB down bandwidths of air resonance of the above openings are shown for a fixed resonance<sup>59</sup> frequency (solid line). The 10-dB-down bandwidth of resonance curve increases monotonically from circular opening to f-hole up to a semitone. The opening area (dotted line), normalized by the area of the present-day f-hole, is reduced by a factor of two from circular opening to c-hole and f-hole.

### Schallabstrahlung altitalienischer Geigen im Vergleich



(c) Meisteratelier für Geigenbau Martin Schleske, Stockdorf 2008

Figure A-17: The sound spectrum of four famous Cremonese violins from Martin Schleske's website [2]. The air resonance at around 270 Hz shows that a 10-dB down bandwidth is more appropriate than the more standard 3-dB down bandwidth.

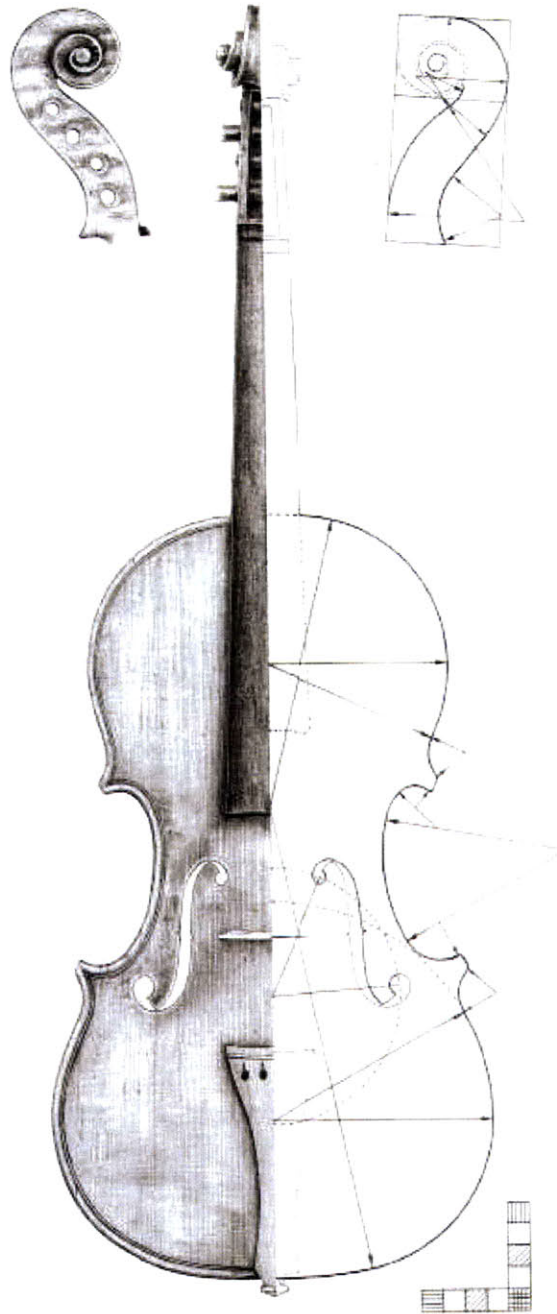


Figure A-18: The drawing of the Emiliani Stradivari of 1703 from which the expression for air resonance frequency is obtained [5].

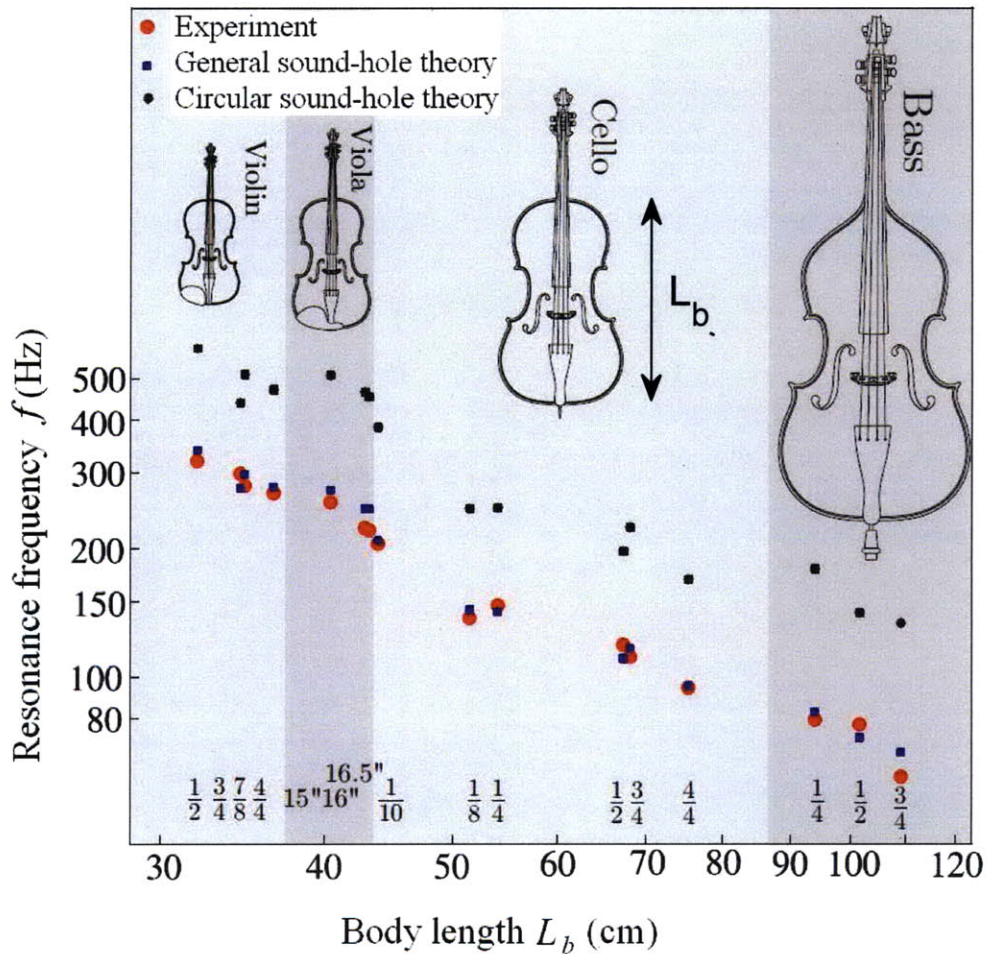


Figure A-19: The effectiveness of the developed approach is shown by applying it to obtain exact air resonance frequency in violin family. The results using general sound-hole theory (in blue) are compared to the results using circular sound-hole theory (in black). A correction factor is used for each member of the family to scale the circular theory data to its corresponding experimental data. The numbers below the figure shows the conventional sizes of each instrument.

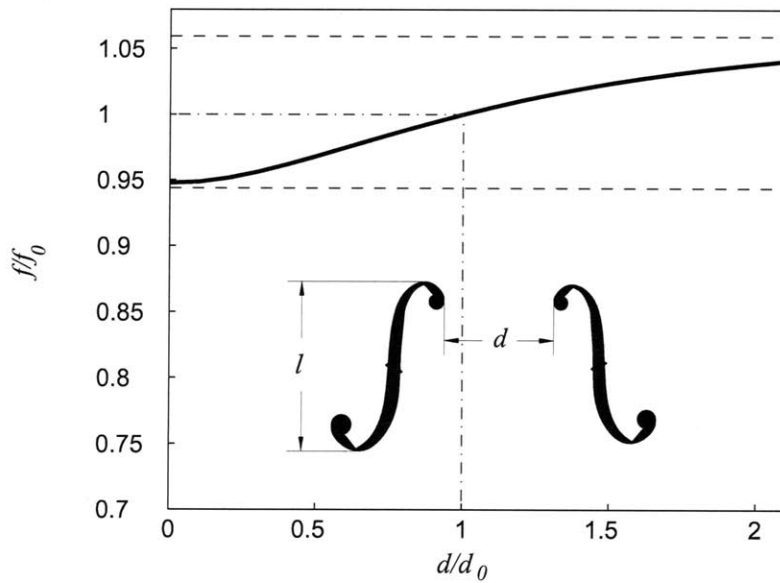


Figure A-20: The effect of the distance between f-holes on air resonance frequency. The resonance frequency  $f$  is normalized by  $f_0$ , the air resonance frequency of an f-hole geometry the same as Stradivari of 1703 (Fig. A-18). The distance  $d$  is normalized by  $d_0$ , the distance between f-holes of the same violin. The horizontal dotted lines shows one semi-tone higher and lower than the reference frequency. The change in distance by a factor of two results in resonance frequency variation of less than a semi-tone.

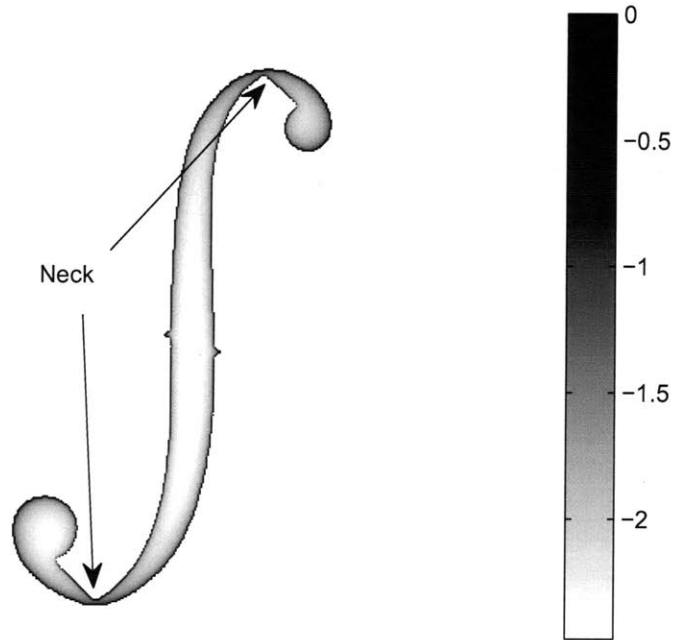


Figure A-21: Flux distribution profile in log scale,  $\log(\sigma)$  (the source strength  $\sigma$  is obtained from Eq. 2.9) is shown for f-hole. The flux is normalized by its maximum value, so the zero value in the colorbar represents the maximum flux value. The irregular shape of f-hole results in higher rate of flux at the necks. The consequent effect is an increase in viscous damping and consequently, an increase in resonance bandwidth. The flux is normalized by the maximum velocity.



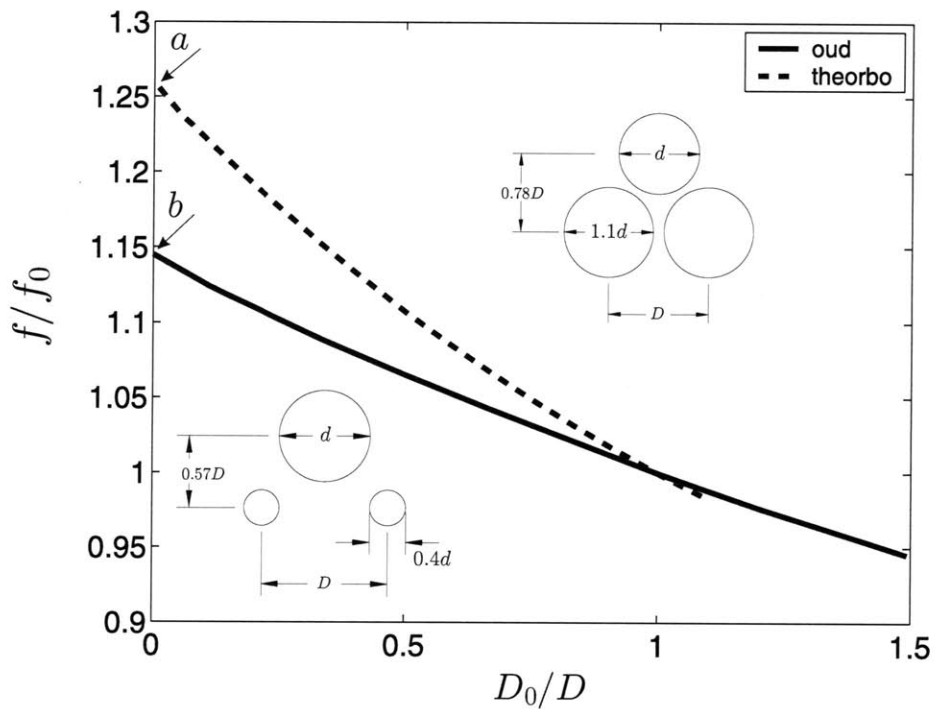


Figure A-22: The distance between the holes  $D$ , normalized by a reference distance  $D_0$  in standard theorbos and ouds, is varying having the hole diameters  $d$  fixed. For theorbo, the upper three circles,  $D_0 = 1.24d$ , and for oud, the lower three circles,  $D_0 = 1.39d$ . The frequencies  $f$  and  $f_0$  represent the corresponding resonance frequencies. The resonance frequencies of theorbo and oud ( $D_0/D = 0$ ), obtained via the developed method, is compared with the superposition approximation, which is equivalent to the case that the holes are infinitely far ( $D_0/D \rightarrow 0$ , shown by the arrows). The lower and upper sketches represent the oud and theorbo sound-holes, respectively. The arrows  $a$  and  $b$  indicate the resonance frequencies when the holes are infinitely far from each other. In this case, using superposition to calculate the resonance frequency is valid.

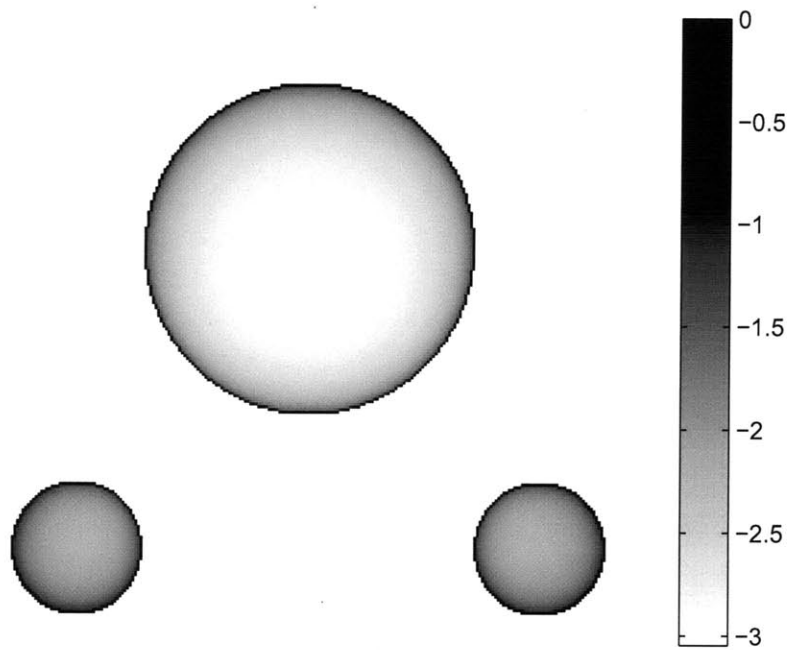


Figure A-23: Flux distribution profile in log scale,  $\log(\sigma)$  (the source strength  $\sigma$  is obtained from Eq. 2.9) is shown for oud sound-hole. The flux is normalized by its maximum value, so the zero value in the colorbar represents the maximum flux value.

# Appendix B

## Tables

Table B.1: The error obtained using Eq. 5.4 based on the semi-empirical Eq. 5.1. Each instrument shown in the table is the one used to find the parameter  $a$  in Eq. 5.1. The resonance frequencies of other instruments of the family is then obtained based the same value of  $a$ .

Instrument	violin			viola		cello			bass	
Size	$\frac{3}{4}$	$\frac{7}{8}$	$\frac{4}{4}$	15"	16"	$\frac{1}{2}$	$\frac{3}{4}$	$\frac{4}{4}$	$\frac{1}{2}$	$\frac{3}{4}$
Error (Hz)	13.77	5.14	5.78	6.19	7.62	6.81	7.59	6.55	5.14	10.89



# Bibliography

- [1] <http://www.lutesandguitars.co.uk/htm/cat06.htm>.
- [2] <http://www.schleske.de/en/our-research/introduction-violin-acoustics/introduction/glossary.html>.
- [3] A. Baines. *The Oxford companion to musical instruments*. Oxford University Press, USA, 1992.
- [4] G. Bissinger. Effect of f-hole shape, area, and position on violin cavity modes below 2 KHz. *Catgu Acoust. Soc. J.*, 2:603–608, 1992.
- [5] K. Coates. *Geometry, proportion and the art of lutherie*. Clarendon Press, 1985.
- [6] L. Cremer. *The physics of the violin*. MIT press, 1984.
- [7] Muller H. Cremer, L. and T. J. Schultz. *Principles and Applications of Room Acoustics, Vol. 1,2* . Applied Science, 1982.
- [8] C. Engel and A.J. Hipkins. *Researches into the early history of the violin family*. Novello, Ewer & co., 1883.
- [9] C.M. Hutchins. A study of the cavity resonances of a violin and their effects on its tone and playing qualities. *The Journal of the Acoustical Society of America*, 87:392, 1990.
- [10] H. Itakawa and C. kumagai. Researches on violin making. *Rep. Inst. industr. Sci. Univ. Tokyo*, 3(1,5), 1952.
- [11] PK Kundu and IM Cohen. *Fluid Mechanics*. 2004.
- [12] H Lamb. *Hydrodynamics*. Dover, 1932.
- [13] H. Lamb. *The dynamical theory of sound*. Dover Pubns, 2004.
- [14] K.D. Marshall. Modal analysis of a violin. *The Journal of the Acoustical Society of America*, 77:695, 1985.
- [15] J. W. S. Rayleigh. *The Theory of Sound*, volume 1. Macmillan, London, 1877–1878. Reprinted by Dover, New York, 1945.

- [16] W. Sandys and S.A. Forster. History of the Violin. *JR Smith, Addison, and Lucas. London*, 1884.
- [17] F. Savart. Memoire sur la construction des Instruments ‘a cordes et ‘a archet (Deterville, Paris 1819). In *Musical Acoustics, Part I (Violin Family Components) and II (Violin Family Functions)*, volume 5-6 of *Benchmark papers in Acoustics*, 1976.
- [18] E. A. G. Shaw. Cavity Resonance in the Violin- Network Reperesentation and effect of damped and undamped rib holes . *Journal of the Acoustical Society of America*, 87(1):398–410, Jan 1990.
- [19] W.M.C. Siebert. *Circuits, signals, and systems*. The MIT Press, 1986.
- [20] E. Van der Straeten. *The History of the Violin, Its ancestors and Collateral Instruments From Earliest Times*. Da Capo Press, 1968.
- [21] G. Vandegrift. Experimental study of the Helmholtz resonance of a violin. *Physica D*, 26:385–395, 1987.
- [22] Hermann L. von Helmholtz. Thoery of Air Oscillations in Tubes with Open ends. *J. Reine Angew. Math.*, 57:1–72, 1860.
- [23] Hermann L. von Helmholtz. *On the Sensations of Tone as a Physiological Basis for the Theory of Music*. Dover, New York, 1954.
- [24] R.H. Wells. Number symbolism in the renaissance lute rose. *Early Music*, 9(1):32–42, 1981.